

Auxiliary Material for paper 2012TC003155

Variable shortening rates in the eastern Himalayan thrust belt, Bhutan: Insights from multiple thermochronologic and geochronologic data sets tied to kinematic reconstructions

Sean P. Long

Nevada Bureau of Mines and Geology, University of Nevada, Reno, Nevada, USA

Nadine McQuarrie

Department of Geology and Planetary Science, University of Pittsburgh, Pittsburgh, Pennsylvania, USA

Tobgay Tobgay

Department of Geological Sciences, University of Texas at El Paso, El Paso, Texas, USA

Isabelle Coutand

Department of Earth Sciences, Dalhousie University, Halifax, Nova Scotia, Canada

Frances J. Cooper

School of Earth and Space Exploration, Arizona State University, Tempe, Arizona, USA

Peter W. Reiners

Department of Geosciences, University of Arizona, Tucson, Arizona, USA

Jo-Anne Wartho and Kip V. Hodges

School of Earth and Space Exploration, Arizona State University, Tempe, Arizona, USA

Long, S. P., N. McQuarie, T. Tobgay, I. Coutand, F. J. Cooper, P. W. Reiners, J.-A. Wartho, and K. V. Hodges (2012), Variable shortening rates in the eastern Himalayan thrust belt, Bhutan: insights from multiple thermochronologic and geochronologic datasets tied to kinematic reconstructions, *Tectonics*, 31, TC5004, doi:10.1029/2012TC003155.

Introduction

Auxiliary Material included for this paper includes Text S1 that contains methods sections, and Figures S1 and S2 and Tables S1-S5 for thermochronometry data sets and 1-D modeling.

1. 2012tc003155-txts01.docx

Text S1. Mineral separation methods of Arizona State University Noble Gas Geochronology and Geochemistry Laboratories 40Ar/39Ar dating, Arizona Radiogenic Helium Dating Laboratory (U-Th)/He dating, Dalhousie University Fission Track Research Laboratory, Arizona LaserChron Center U/Pb zircon dating, and of 1-D exhumation rate modeling.

2. 2012tc003155-fs01a.jpg, 2012tc003155-fs01b.jpg

Figure S1. 40Ar/39Ar age spectra and inverse isochron plots. Inverse isochron plots and age spectra plots for analyses that involved more than two heating steps are shown. Individual age spectra plots for BU07-22 are shown for all heating steps and for low-temperature steps.

3. 2012tc003155-fs02a.jpg, 2012tc003155-fs02b.jpg, 2012tc003155-fs02c.jpg, 2012tc003155-fs02d.jpg, 2012tc003155-fs02e.jpg

Figure S2. Temperature-time (T-t) graphs for all eastern Bhutan samples. The blue swath illustrates permissible variability between successive T-t datapoints, and accounts for ranges of peak temperature, ranges of closure temperature, and cooling age uncertainty. Black numbers indicate exhumation rates (mm/yr) for a 30°C/km geothermal gradient, and gray numbers indicate the total permissible range of exhumation rates for given age uncertainties, closure temperature ranges, and modeled geothermal gradients (20°C and 40°C/km).

4. 2012tc003155-ts01.xls

Table S1. White mica 40Ar/39Ar data.

5. 2012tc003155-ts02.xlsx

Table S2. Single-grain zircon (U-Th)/He ages and supporting data.

6. 2012tc003155-ts03.xlsx

Table S3. Apatite fission-track data: rho's, spontaneous track density;

N_s, number of spontaneous tracks counted; rho_i, induced track density in external detector (muscovite); N_i, number of induced tracks counted; rho_d, induced track density in external detector adjacent to dosimetry glass; N_d, number of tracks counted in determining rho_d; P(Chi_2), chi-square probability.

7. 2012tc003155-ts04.xlsx

Table S4. U-Pb (zircon) geochronologic analyses by laser-ablation multicollector ICP mass spectrometry.

8. 2012tc003155-ts05.xlsx

Table S5. Data table showing results from exhumation rate modeling.

Yellow highlighted cells indicate closure temperature range and exhumation rates (from closure temperature to surface) calculated from AGE2EDOT modeling, orange highlighted cells indicate exhumation rates calculated manually between time of achievement of peak temperature and highest-temperature thermochronometer, and green highlighted cells indicate exhumation rates between each temperature-time data point for a given sample, for all three geothermal gradients, which were used to calculate the T-t paths in Figs. 7 and S2.

1 **Text S1**

2

3 **Section 1: Mineral separation methods**

4

5 Standard mineral separation procedures were used to obtain zircon, apatite, and
6 muscovite fractions from all rock samples. This included crushing and pulverizing whole rock
7 samples to sand-size grains, followed by density separation on a Wilfley table, separation into
8 dense and light fractions by heavy liquid separation, and passing the dense fraction through a
9 Frantz magnetic separator.

10

11 **Section 2: Methods of Arizona State University Noble Gas Geochronology and**

12 **Geochemistry Laboratories $^{40}\text{Ar}/^{39}\text{Ar}$ dating**

13

14 White mica grains from samples BU07-6, BU07-9, BU07-11, BU07-12, BU07-21,
15 BU07-22, BU07-29, and NBH-11 were handpicked, cleaned in acetone, methanol, and deionized
16 water, and individually wrapped in aluminum foil packets. For the irradiation package, sample
17 packets were regularly interspersed with packets of biotite age standard HD-B1 (24.18 ± 0.09 Ma;
18 Schwarz and Trieloff, 2007) to monitor the neutron flux gradient, along with synthetic Ca and K
19 salts to determine interfering nuclear production ratios. The ca. 16 mm diameter aluminum disks
20 (containing holes for 7 samples and standards) into which the packets were loaded were stacked
21 and secured together to make up the irradiation package, which was Cd foil shielded and
22 irradiated for 1.2 hours at a near-core position (5C) within the McMaster University nuclear
23 reactor, Hamilton, Ontario, Canada.

24 Upon return, individual age standard grains and multi-grain samples were loaded into a
25 61 mm diameter aluminum palette containing a series of 2x2x2 mm holes. The palette and a
26 glass coverslip were loaded into an ultra-high vacuum 4.5" laser chamber with a Kovar glass
27 viewport and baked and pumped at 120°C for one day, followed by turbo-pumping for an
28 additional day to remove adsorbed atmospheric argon from the samples and chamber walls.

29 To step-heat each multi-grain sample, a 60 W IPG Photonics infrared (970 nm) diode
30 laser, with computer-controlled Photon Machines optics and X-Y-Z stages linked to a Newport
31 controller, was used. For the laser step-heating procedure, the laser was fired for two minutes

32 using a 4 mm fixed laser beam diameter from 5-9.3 W, and a 0.6 mm jogging laser beam
33 diameter from 15-50 W, to ensure total fusion of the samples. The number of steps was selected
34 based on the quantity of sample available (note that there was very little material for some of
35 these samples), and the estimated ages and %K contents. The gases released by laser heating
36 were purified for an additional two minutes using two SAES NP10 getter pumps (one at 400°C
37 and one at room temperature) to remove all active gases. The remaining gases were equilibrated
38 into a high sensitivity multi-collector mass spectrometer (Nu Instruments Noblesse), containing a
39 Nier-type source operated at 400 mA. The Ar isotopes were measured using a 1×10^{11} Ohm
40 Faraday detector or an ETP ion counting multiplier, depending upon the ^{40}Ar signal size.
41 Detector intercalibration for ^{40}Ar was performed using multiple air shots. Laser heating, X-Y
42 stage movement, automated valve operation, and data acquisition was automated and computer
43 controlled using the Mass Spec software program.

44 The mean 4 minute extraction system cold blank Ar isotope measurements obtained
45 during the experiments were 1.27×10^{-16} , 2.04×10^{-18} , 2.59×10^{-19} , 1.96×10^{-18} , and 9.17×10^{-19}
46 moles STP (standard temperature and pressure) for samples BU07-6, BU07-21 and BU07-22,
47 1.11×10^{-16} , 2.49×10^{-18} , 2.52×10^{-19} , 2.17×10^{-18} , and 1.01×10^{-18} moles STP for samples
48 BU07-9, BU07-11 and NBH-11, and 8.14×10^{-17} , 1.27×10^{-18} , 1.27×10^{-19} , 1.22×10^{-18} , and
49 5.15×10^{-19} moles STP for samples BU07-12 and BU07-29, for ^{40}Ar , ^{39}Ar , ^{38}Ar , ^{37}Ar , and ^{36}Ar ,
50 respectively. Where appropriate, 15 and 50 W hot blanks were also analyzed at the end of each
51 sample laser step-heating procedure to check for potential larger blank contributions from melted
52 sample interaction with the glass coverslip, and these blank values were 1.05×10^{-16} , 2.82×10^{-18} ,
53 2.54×10^{-19} , 2.42×10^{-18} , and 9.07×10^{-19} moles STP for sample BU07-9 (15 W), 9.97×10^{-17} ,
54 3.42×10^{-18} , 2.63×10^{-19} , 2.12×10^{-18} , and 8.15×10^{-19} moles STP for sample BU07-11 (15 W),
55 9.06×10^{-17} , 1.95×10^{-18} , 1.69×10^{-19} , 1.54×10^{-18} , and 6.15×10^{-19} moles STP for sample BU07-
56 12 (15 W), 1.70×10^{-15} , 2.50×10^{-18} , 2.76×10^{-19} , 2.17×10^{-18} , and 8.43×10^{-19} moles STP for
57 sample BU07-21 (15 W), $1.26-1.35 \times 10^{-16}$, $2.09-2.18 \times 10^{-18}$, $2.23-2.98 \times 10^{-19}$, $1.92-2.21 \times 10^{-18}$,
58 and $8.77-8.87 \times 10^{-19}$ moles STP for sample BU07-22 (15 and 50 W), and 9.45×10^{-17} , $2.31 \times$
59 10^{-18} , 2.60×10^{-19} , 1.54×10^{-18} , and 6.15×10^{-19} moles STP for sample NBH-11(15 W),
60 for ^{40}Ar , ^{39}Ar , ^{38}Ar , ^{37}Ar , and ^{36}Ar , respectively. The sensitivities of the Faraday and ion
61 counting detectors were 9.523×10^{-13} moles/V and 1.595×10^{-20} moles/cps, respectively.

62 ^{40}Ar measurements made on the Faraday detector were converted to ^{40}Ar ion counting
63 detector values (i.e., cps) using an intercalibration factor obtained from appropriately-sized air
64 shots in which both the ^{40}Ar Faraday and ion-counting detector signals were measured.
65 Therefore, multiple air shots (consisting of 1-5 air pipette slugs of gas) were analyzed throughout
66 the unknown analyses. Unknown analyses were also corrected for mass spectrometer
67 discrimination using air shots. The measured $^{40}\text{Ar}/^{36}\text{Ar}$ air ratios varied from 287.21 ± 2.48 to
68 307.50 ± 1.80 (1σ errors) during the 6 days of analyses of samples BU07-6, BU07-21 and BU07-
69 22, 290.45 ± 1.56 to 297.58 ± 1.14 for the 8 days of analyses of samples BU07-9, BU07-11 and
70 NBH-11, and 288.49 ± 1.63 to 300.20 ± 1.18 for the 6 days of analyses of samples BU07-12 and
71 BU07-29. Nuclear interference correction factors were as follows: $^{40}\text{Ar}/^{39}\text{Ar}_K =$
72 0.027945 , $^{36}\text{Ar}/^{38}\text{Ar}_{\text{Cl}} = 316$, $\text{Ca}/K = 1.92234$, and $\text{Cl}/K = 0.16863$. Errors throughout this paper
73 are quoted at the 2σ confidence level. $^{40}\text{Ar}/^{39}\text{Ar}$ ages were calculated using the decay constant,
74 branching ratio, and atmospheric $^{40}\text{Ar}/^{36}\text{Ar}$ ratio recommended by Steiger and Jäger (1977). J-
75 values and errors are noted in Table S1.

76 Supporting data for $^{40}\text{Ar}/^{39}\text{Ar}$ analyses are shown in Table AM1, and $^{40}\text{Ar}/^{39}\text{Ar}$ inverse
77 isochron and age spectra plots are shown in Fig. S1. Final interpreted $^{40}\text{Ar}/^{39}\text{Ar}$ ages for each
78 sample are shown in Table 1 in the text, and data used in interpretation of these ages are shown
79 in Table 2 in the text.

80

81 **Table S1: White mica $^{40}\text{Ar}/^{39}\text{Ar}$ data:**

82

83

84 **Figure S1: $^{40}\text{Ar}/^{39}\text{Ar}$ age spectra and inverse isochron plots:** Inverse isochron plots and age
85 spectra plots for analyses that involved more than two heating steps are shown. Individual age
86 spectra plots for BU07-22 are shown for all heating steps and for low-temperature steps.

87

88

89

90 **Section 3: Methods of Arizona Radiogenic Helium Dating Laboratory (U-Th)/He dating**

91

92 Zircon (U-Th)/He analyses followed the general procedures outlined in Reiners et al.
93 (2004) and Reiners (2005). Individual zircon grains were selected from separates on the basis of
94 size, morphology, and lack of inclusions. Grains lacking obvious fractures and with a minimum
95 radius of 60 μm , with minimal to no inclusions, were selected. The dimensions of individual
96 grains were measured from digital photomicrographs, using the approach outlined in Hourigan et
97 al. (2005) for alpha-ejection corrections. Single grains were then packed into 1-mm Nb foil
98 envelopes. Multiple foil packets were then placed in individual holes in a 30-hole planchett
99 inside a ~7-cm laser cell pumped to $<10^{-9}$ torr. Individual packets were then heated for 15
100 minutes by a focused beam of a 1-2 W laser, to extract ${}^4\text{He}$. The packets were then re-heated for
101 15 minutes, often multiple times, until ${}^4\text{He}$ yields were less than 1% of total. Standards of Fish
102 Canyon Tuff (FCT) zircon (28.48 ± 0.06 Ma [2σ], Schmitz and Bowring [2001]) were analyzed
103 between every 5 unknowns.

104 Gas released from heated samples was spiked with 0.1-0.2 pmol ${}^3\text{He}$, and condensed onto
105 activated charcoal at the cold head of a cryogenic trap at 16 K. Helium was then released from
106 the cold head at 37 K into a small volume (~50 cc) with an activated Zr-Ti alloy getter and the
107 source of a Balzers quadrupole mass spectrometer (QMS) with a Channeltron electron multiplier.
108 Peak-centered masses at approximately m/z of 1, 3, 4, and 5.2 were measured. Mass 5.2
109 establishes background, and mass 1 is used to correct mass 3 for HD and H $3+$. Corrected ratios
110 of masses 4 to 3 were regressed through ten measurement cycles over ~15 s to derive an intercept
111 value, which has an uncertainty of 0.05-0.5% over a ${}^4\text{He}/{}^3\text{He}$ range of ~ 10^3 , and compared with
112 the mean corrected ratio to check for significant anomalous changes in the ratio during analysis.
113 Helium contents of unknown samples were calculated by first subtracting the average mass-1-
114 corrected ${}^4\text{He}/{}^3\text{He}$ measured on multiple procedural blanks analyzed by the same method, from
115 the mass-1-corrected ${}^4\text{He}/{}^3\text{He}$ measured on the unknown. This was then ratioed to the mass-1-
116 corrected ${}^4\text{He}/{}^3\text{He}$ measured on a shot of an online reference ${}^4\text{He}$ standard analyzed with the
117 same procedure. The resulting ratio of measured ${}^4\text{He}/{}^3\text{He}$ values was then multiplied by the
118 moles of ${}^4\text{He}$ delivered in the reference shot.

119 After He extraction and measurement, foil packets were retrieved, transferred to Teflon
120 vials, and spiked with 0.5-1.0 ng of ${}^{233}\text{U}$ and ${}^{229}\text{Th}$. High-pressure digestion vessels were used
121 for dissolution of the zircon and Nb foil packet. Natural-to-spike isotope ratios of U and Th were
122 then measured on a high-resolution (single-collector) Element2 ICP-MS with all-PFA Teflon

123 sample introduction equipment and sample preparation/analytical equipment. Blanks for zircon
124 analyses were 2.6 ± 0.5 pg U and 5.5 ± 1.0 pg Th. Precision on measured U-Th ratios is typically
125 better than 0.5% for zircon analyses. Propagated analytical uncertainties for typical zircon
126 samples led to an estimated analytical uncertainty on (U-Th)/He ages of approximately 1-3%
127 (1σ). In some cases, reproducibility of multiple aliquots approaches analytical uncertainty.
128 However, in general, reproducibility of repeat analyses of (U-Th)/He ages is significantly worse
129 than analytical precision. Thus (U-Th)/He ages typically show a much greater scatter and higher
130 MSWD than expected based on analytical precision alone, and multiple replicate analyses of (U-
131 Th)/He ages on several aliquots is necessary for confidence in a particular sample age.

132 For further information on the methods of (U-Th)/He dating at the Arizona Radiogenic
133 Helium Dating Laboratory, refer to Reiners (2005), or to the laboratory's
134 website: <http://www.geo.arizona.edu/~reiners/arhdl/arhdl.htm>. Single-grain ZHe ages and
135 supporting data are shown on Table S2, and weighted mean ZHe ages for each sample are shown
136 on Table 1 in the text.

137

138

139 **Table S2: Single-grain zircon (U-Th)/He ages and supporting data**

140

141

142

143 **Section 4: Methods of the Dalhousie University Fission Track Research Laboratory**

144

145 Apatites were mounted in araldite epoxy on glass slides, ground and polished to expose
146 internal grain surfaces, then etched for 20 seconds in 5.5M HNO₃ to reveal spontaneous fission
147 tracks. All the mounts were prepared using the external detector method (EDM; Hurford and
148 Green, 1983; for a summary, see also Gallagher et al., 1998). Samples and CN-5 glass standards
149 were irradiated at the Oregon State University reactor. The low-U muscovite external detectors
150 that covered the apatite grain mounts and CN-5 glass dosimeter were etched in 40% HF for 45
151 minutes at 21°C to reveal induced fission tracks. Samples were analysed with a Zeiss Axioplan
152 microscope at x1000 magnification attached to a Kinetek computer-controlled high-precision
153 stage driven by the FTStage program (Dumitru, 1993). Fission-track ages were calculated using

154 a weighted mean zeta calibration (Hurford and Green, 1983) based on IUGS age standards
155 (Durango, Fish Canyon and Mount Dromedary apatites) (Miller et al., 1985; Hurford, 1990). All
156 samples processed by I. Coutand with a ζ value based on 23 analyses $\zeta = 370.6 \pm 5$ for dosimeter
157 glass CN5.

158 Supporting data for AFT analyses are shown on Table S3, and AFT ages are reported on
159 Table 1 in the text.

160

161

162 **Table S3: Apatite fission-track data:** ρ_s , spontaneous track density; N_s , number of spontaneous
163 tracks counted; ρ_i , induced track density in external detector (muscovite); N_i , number of induced
164 tracks counted; ρ_d , induced track density in external detector adjacent to dosimetry glass; N_d ,
165 number of tracks counted in determining ρ_d ; $P(\chi^2)$, chi-square probability.

166

167

168

169 **Section 5: Methods of Arizona LaserChron Center U/Pb zircon dating**

170

171 Zircon separates from BU07-42 were mounted on two-sided tape, on top of an epoxy
172 mount. Photographic images were made of this zircon mount to keep track of which grains were
173 dated.

174 Material was ablated from each zircon surface using a DUV193 Excimer laser system
175 from New Wave Instruments. The laser operates at a wavelength of 193 nm, and for the
176 analyses in this study a 15 micron-wide spot size was used (see footnotes of Table S4). For most
177 analyses the laser was operated at minimum output energy (~40 mJ) with a repetition rate of 8
178 pulses per second, which created a ~15 micron-deep pit for a typical 20 second analysis. The
179 ablated material is carried in helium gas into the plasma source of a multicollector inductively
180 coupled plasma mass spectrometer (an Isoprobe, from GV Instruments). This instrument is
181 equipped with nine moveable Faraday collectors and four low-side Channeltrons (ion counters).
182 Eight of the Faraday collectors use a 10^{11} ohm resistor, whereas the Faraday used for
183 measuring ^{207}Pb is equipped with a 10^{12} ohm resistor. This configuration allows static-mode
184 measurement of all isotopes, using 10^{11} Faraday detectors for ^{238}U , ^{232}Th , ^{208}Pb , and ^{206}Pb , a 10^{12}

185 Faraday detector for ^{207}Pb , and an ion-counting channel for ^{204}Pb . Each analysis consists of one
186 20-second integration on peaks with the laser off (for backgrounds), 20 or 12 one-second
187 integrations with the laser firing, and a 30 second delay to purge the previous sample and prepare
188 for the next analysis. Each analysis is evaluated for consistency of $^{206}\text{Pb}/^{238}\text{U}$ and $^{206}\text{Pb}/^{207}\text{Pb}$
189 ratios through the 20 seconds of data acquisition. If ratios display either a sudden change, or a
190 gradual increase greater than ~5% for $^{206}\text{Pb}/^{238}\text{U}$, the analysis is discarded. This ensures that
191 analyses are not compromised by crossing an age boundary.

192 Common Pb correction was accomplished by using the measured ^{204}Pb and assuming an
193 initial Pb composition from Stacey and Kramers (1975). Conservative uncertainties of 1.0
194 for $^{206}\text{Pb}/^{204}\text{Pb}$, 0.3 for $^{207}\text{Pb}/^{204}\text{Pb}$, and 2.0 for $^{208}\text{Pb}/^{204}\text{Pb}$ were used for the composition of the
195 common Pb. ^{204}Hg present in the argon plasma gas, as well as any background ^{204}Pb or
196 molecular 204, was accounted for by first measuring backgrounds in the 204 mass position, then
197 measuring the peak 204 intensity with the laser firing, and subtracting the background intensity
198 from the peak intensity.

199 Fractionation of Pb/U and Pb/Th occurs primarily in the laser pit, and is highly sensitive
200 to the rate of carrier gas flow across the sample surface. An optimal balance between signal
201 intensity and stability occurs at a carrier gas flow rate of 0.45 ml/minute, which generates a Pb/U
202 sensitivity of 0.9 (e.g., a 500 Ma zircon yields a $^{206}\text{Pb}/^{238}\text{U}$ age of 450 Ma). To correct for Pb/U
203 and Th/U fractionation, standards were analyzed once every 5 unknowns. Fractionation
204 standards for zircon are fragments of a large Sri Lanka zircon crystal that yields an age of
205 563.5 ± 3.2 Ma (2σ , ID-TIMS) (Gehrels et al., 2008). The unknowns are corrected for the closest
206 6 standards using a sliding window average. The error on this fractionation factor is generally
207 ~1% (2σ) for $^{206}\text{Pb}/^{238}\text{U}$ ages. Fractionation of Pb isotopes is minimal, with a maximum of ~3%
208 fractionation of $^{206}\text{Pb}/^{207}\text{Pb}$. This fractionation is also removed by comparison with standards,
209 using the same procedure described above. The error on this fractionation factor is generally
210 ~1% (2σ) for $^{206}\text{Pb}/^{207}\text{Pb}$ ages. Pb/U and Pb/Th fractionation varies with depth during laser
211 ablation, increasing by ~5% during a 20-second analysis that excavates to a depth of 15 microns.
212 This was accounted for by monitoring the depth-related fractionation of standards, and then
213 applying a sliding-window depth-related fractionation factor to the unknowns. Pb/U
214 fractionation also varies by up to several percent depending on position on the mount surface,
215 due to variations in the flow rate/pattern of the helium carrier gas across the sample surface. For

216 this reason, all standards and unknowns are mounted close together in the central portion of the
217 mount, and care was taken to analyze standards that are as close as possible to each unknown.

218 To determine accurate concentrations of U and Th, intensities are compared with the Sri
219 Lanka standard, which has concentrations of U, Th, and Pb known to ~20%. For each zircon
220 analysis, the errors in determination of $^{206}\text{Pb}/^{238}\text{U}$ and $^{206}\text{Pb}/^{204}\text{Pb}$ result in a measurement error
221 of ~1-2% (at 2σ level) in the $^{206}\text{Pb}/^{238}\text{U}$ age. The errors in measurement of $^{206}\text{Pb}/^{207}\text{Pb}$
222 and $^{206}\text{Pb}/^{204}\text{Pb}$ also result in ~1-2% (at 2σ level) uncertainty in age for grains that are >1.0 Ga,
223 but are substantially larger for younger grains due to low intensity of the ^{207}Pb signal. Errors that
224 arise from the measurement of $^{206}\text{Pb}/^{238}\text{U}$, $^{206}\text{Pb}/^{207}\text{Pb}$, and $^{206}\text{Pb}/^{204}\text{Pb}$ are referred to as random
225 (or measurement) errors, because they are different for each analysis within a session. For most
226 analyses, the cross-over in precision of these random errors for $^{206}\text{Pb}/^{238}\text{U}$ and $^{206}\text{Pb}/^{207}\text{Pb}$ ages
227 occurs at ~1.0 Ga. For this reason, $^{206}\text{Pb}/^{238}\text{U}$ ratios were considered the most representative,
228 and were used for analyses younger than ~1.0 Ga, and $^{207}\text{Pb}^*/^{206}\text{Pb}^*$ ratios were considered the
229 most representative, and were used for ages older than ~1.0 Ga. Table S4 shows the cutoff ages
230 used for individual samples; these cutoff ages were chosen as close to ~1.0 Ga as possible
231 without dividing an age peak artificially (for example, for an age cluster between 900-1050 Ma,
232 cutoff would be at 1060 Ma, or for a cluster between 1000-1200 Ma, cutoff would be at 980 Ma).

233 Data table S4 reports analytical data at 1σ uncertainties based on the analytical (or
234 measurement) errors. For determination of the age of metamorphic rim growth in sample BU07-
235 42, (see sections 4.4 and 5.3 in the text for further discussion), we used the weighted mean age
236 from Ludwig (2003) of the 17 youngest analyses that cluster closely in age and overlap the
237 concordia line (total age range is 14.1 ± 0.7 Ma to 21.0 ± 0.7 Ma [1σ]), which is 17.2 ± 0.3 Ma (2σ
238 internal error). The youngest permissible age for growth of metamorphic zircon rims, as defined
239 by the weighted mean age from Ludwig (2003) of the youngest 3 concordant analyses that
240 overlap in age (within error; 14.1 ± 0.7 Ma, 15.0 ± 0.4 Ma, and 15.2 ± 0.5 Ma), is 14.9 ± 0.6 Ma (2σ
241 internal error). The uncertainty of the weighted mean is based on the scatter and precision of the
242 set of concordant ages, weighted according to their measurement errors. Systematic errors
243 include contributions from the fractionation correction, composition of common Pb, age of the
244 calibration standard, and U decay constants. The total average systematic errors for BU07-42 are
245 2.5% for $^{206}\text{Pb}/^{238}\text{U}$, and 3.5% for $^{206}\text{Pb}/^{207}\text{Pb}$. Quadratic addition of the measurement and
246 systematic ($^{206}\text{Pb}/^{238}\text{U}$) errors for this sample yield final reported weighted mean ages of

247 17.2±0.5 Ma (2 σ) for the coherent group of the youngest 17 grains, and 14.9±0.7 Ma (2 σ) for the
248 youngest 3 grains. The average $^{206}\text{Pb}/^{238}\text{U}$ age for all standards run while analyzing sample
249 BU07-42 is 565±14 Ma (1 σ).

250 Data from analyzed zircons from BU07-42 were plotted on Pb/U concordia diagrams
251 using algorithms of Ludwig (2003) (Fig. 6 in the text). Interpretations of the significance of
252 U/Pb zircon ages are based on the view that only clusters of ages record robust sources ages.
253 This is because a single age determination may be compromised by Pb-loss or inheritance (even
254 if concordant), whereas it is unlikely that two or more grains that have experienced Pb loss or
255 inheritance would yield the same age. We accordingly attach age significance only to clusters
256 defined by three or more analyses that overlap in age within error.

257 For further discussion of the analytical methods of the University of Arizona LaserChron
258 Center, please refer to the laboratory website
259 (<https://sites.google.com/a/laserchron.org/laserchron/>), and to Gehrels et al. (2006; 2008).

260
261

262 **Table S4:** U-Pb (zircon) geochronologic analyses by laser-ablation multicollector ICP mass
263 spectrometry.

264
265
266
267

268 **Section 6: Methods of 1-D exhumation rate modeling**

269

270 We used the AGE2EDOT program (Brandon et al., 1998) to quantify the permissible
271 range of exhumation rates required to obtain the observed cooling ages. Our rationale for this 1-
272 D thermal modeling approach follows the detailed justification presented in Thiede et al. (2009),
273 which is based on the results of Whipp et al. (2007), who found that cooling ages are the most
274 sensitive to the vertical (i.e., 1-D exhumation) component of the kinematic field in rapidly-
275 eroding orogens, and the application of models (Ehlers et al., 2005; Reiners and Brandon, 2006)
276 suggesting minimal effects of thermal transients on the rapid exhumation rates typical to the
277 Himalaya.

278 The modeling was used to identify the permissible range of exhumation rates required to
279 obtain the MAr, ZHe, and AFT cooling ages. This was performed by inputting estimates for
280 thermo-physical properties of Himalayan rocks for individual models for each
281 thermochronometer. Input model parameters included: 1) Thermal diffusivity (κ), which was
282 varied between 21, 38, and 48 km^2/myr , which correspond to thermal conductivity values of
283 1.531, 2.770, and 3.498 W/mK , respectively. These represent the low, center, and high values of
284 the 1.5-3.5 W/mK range of thermal conductivity estimated for Himalayan rocks (Ray et al.,
285 2007; Herman et al., 2010), and the center of the 2.5-3.0 W/mK thermal conductivity range
286 estimated by Whipp et al. (2007). 2) Uniform internal heat production rate (H_T), which was
287 varied between 11, 26, and $33^\circ\text{C}/\text{myr}$, which corresponds to volumetric heat production values
288 of 0.802, 1.895, and $2.405 \mu\text{W/m}^3$, respectively. These represent the low, center and high values
289 of the 0.8-2.4 $\mu\text{W/m}^3$ volumetric heat production estimated for LH rocks (Herman et al., 2010).
290 3) For layer depth to constant temperature (L), a value of 30 km was used, based on petrologic
291 estimates for the peak depth of GH rocks in Bhutan (Daniel et al., 2003; Corrie et al., 2012). 4)
292 For surface temperature (T_s), 20°C , the average surface temperature of the town of Mongar in
293 eastern Bhutan
294 (http://www.nepaltravels.com/bhutan/general_information/weather_climate.htm) was used. 5)
295 Three surface thermal gradients (G_T) were modeled: 20, 30, and 40°C/km . This parameter was
296 the largest unknown, because data directly constraining the geothermal gradient in Bhutan are
297 not available. Petrologic estimates of peak temperatures and pressures obtained from GH rocks
298 in eastern and central Bhutan indicate that geothermal gradients may have been as low as ca. 20-
299 25°C/km at ca. 22 Ma (Daniel et al., 2003; Corrie et al., 2012). However, since nearly all of our
300 cooling ages come from LH rocks, and are much younger (ca. 16-3 Ma total range), we
301 cautiously chose to model a large range of geothermal gradients (20-40 C/km) in the absence of
302 more direct constraints. The effects of these different geothermal gradients had the most
303 significant effect on the permissible range of exhumation rates, and far outweighed the effects of
304 varying thermal diffusivity (thermal conductivity) and internal heat production (volumetric heat
305 production).

306 Estimates for the peak temperature range for each sample, and any available timing
307 constraints for achieving peak temperature for GH, LH, and TH rocks in eastern Bhutan were
308 also incorporated into the T-t paths. These data include petrologic estimates for peak

309 temperature and monazite geochronology for GH rocks and lower LH rocks just below the MCT
310 (Daniel et al., 2003), petrologic estimates for peak temperature and monazite geochronology
311 from the Chekha Formation (Kellett et al., 2010; Chambers et al., 2011), deformation
312 temperature ranges for all thrust sheets comprised of LH rocks in eastern Bhutan (Long et al.,
313 2011c), peak temperature data from raman spectroscopy on carbonaceous material (RSCM) for
314 the ST sheet and multiple Baxa Group horses on the Trashigang transect (Whynot et al., 2010),
315 peak temperature constraints from cooling ages presented in this study (e.g., reset [syn-
316 Himalayan] vs. non-reset [Proterozoic] MAr ages), and timing constraints for achieving peak
317 temperature from this study (e.g., timing of growth of metamorphic zircon rims in the Baxa
318 Group; see sections 4.4 and 5.3 in the text).

319 Temperature-time (T-t) graphs were constructed for each of our 32 samples, using the 7
320 new MAr ages, 32 new ZHe ages, and 7 new AFT ages presented in this paper. In addition,
321 published cooling ages, including 4 MAr ages and 1 AFT age from Stüwe and Foster (2001), 15
322 AFT ages from Grujic et al. (2006), and 1 MAr age from Kellett et al. (2009) (Fig. 2), were
323 utilized to augment the T-t paths for 6 of our samples, and to generate 4 additional T-t paths. All
324 36 T-t paths are shown in Fig. S2, and data used in their construction are shown in Table S5. For
325 each T-t path, a range of exhumation rates was calculated between the temperature and timing
326 range of peak conditions and the highest-temperature thermochronologic system for each sample,
327 and the permissible range of exhumation rates between each thermochronologic system and
328 between the lowest-temperature thermochronologic system and the surface (20°C at 0 Ma) was
329 estimated using the AGE2EDOT modeling results. Temperature errors were obtained from the
330 upper and lower limits of the peak temperature range for each sample and from the closure
331 temperature range for each thermochronometer estimated by AGE2EDOT modeling. These
332 were incorporated along with uncertainty for the timing that the sample achieved peak
333 temperature and for uncertainty in cooling ages to make the blue swath, which shows the
334 permissible variation in the T-t path. For each segment of the T-t path between successive
335 datapoints, the exhumation rate (mm/yr) for a 30°C/km geothermal gradient and the center age is
336 shown in black text. The gray text indicates the permissible range in exhumation rates for a
337 40°C/km geothermal gradient and the high age error bar (low exhumation rates) and a 20°C/km
338 geothermal gradient and the low age error bar (high exhumation rates).
339

340

341 **Table S5:** Data table showing results from exhumation rate modeling. Yellow highlighted cells
342 indicate closure temperature range and exhumation rates (from closure temperature to surface)
343 calculated from AGE2EDOT modeling, orange highlighted cells indicate exhumation rates
344 calculated manually between time of achievement of peak temperature and highest-temperature
345 thermochronometer, and green highlighted cells indicate exhumation rates between each
346 temperature-time data point for a given sample, for all three geothermal gradients, which were
347 used to calculate the T-t paths in Figs. 7 and S2.

348

349

350 **Figure S2:** Temperature-time (T-t) graphs for all eastern Bhutan samples. The blue swath
351 illustrates permissible variability between successive T-t datapoints, and accounts for ranges of
352 peak temperature, ranges of closure temperature, and cooling age uncertainty. Black numbers
353 indicate exhumation rates (mm/yr) for a 30°C/km geothermal gradient, and gray numbers
354 indicate the total permissible range of exhumation rates for given age uncertainties, closure
355 temperature ranges, and modeled geothermal gradients (20° and 40°C/km).

356

357

358 **References cited:**

359

360 Brandon, M. T., M. K. Roden-Tice, and J. I. Garver (1998), Late Cenozoic exhumation of the
361 Cascadia accretionary wedge in the Olympic Mountains, northwest Washington State, *Geol. Soc.
362 Am. Bull.*, 110, 985–1009, doi:10.1130/0016-7606(1998)110<0985:LCEOTC>2.3.CO;2.

363

364 Chambers, J., R. Parrish, T. Argles, N. Harris, and M. Horstwood (2011), A short-duration pulse
365 of ductile normal shear on the outer South Tibetan detachment in Bhutan: Alternating channel
366 flow and critical taper mechanics of the eastern Himalaya, *Tectonics*, 30, TC2005,
367 doi:10.1029/2010TC002784.

368

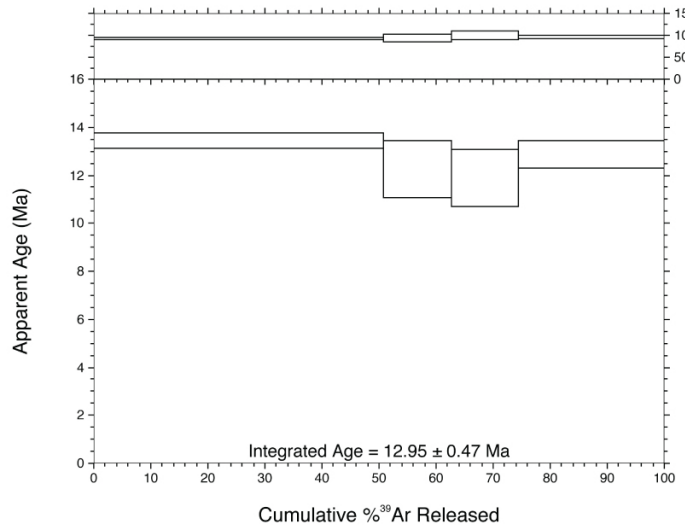
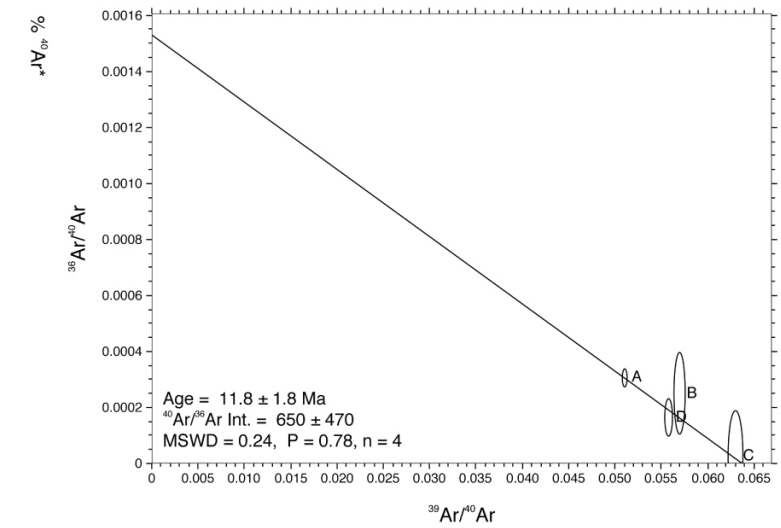
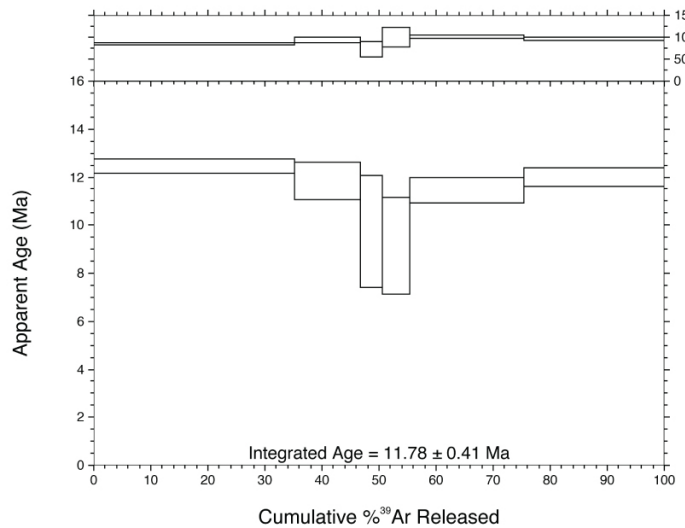
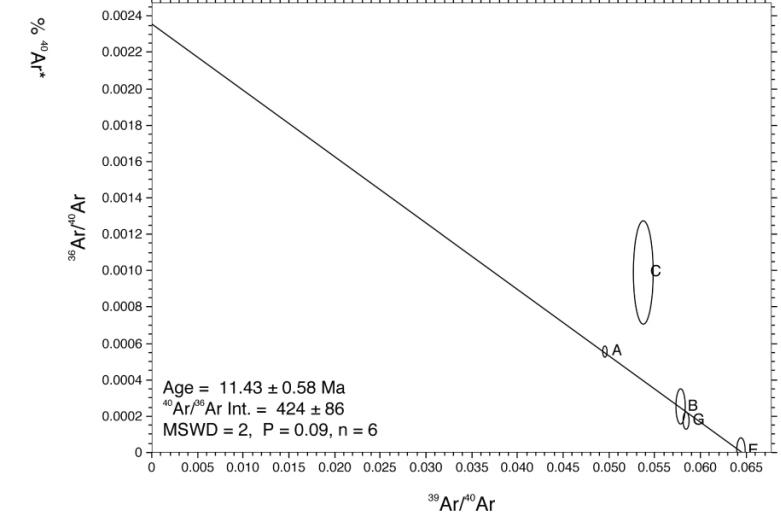
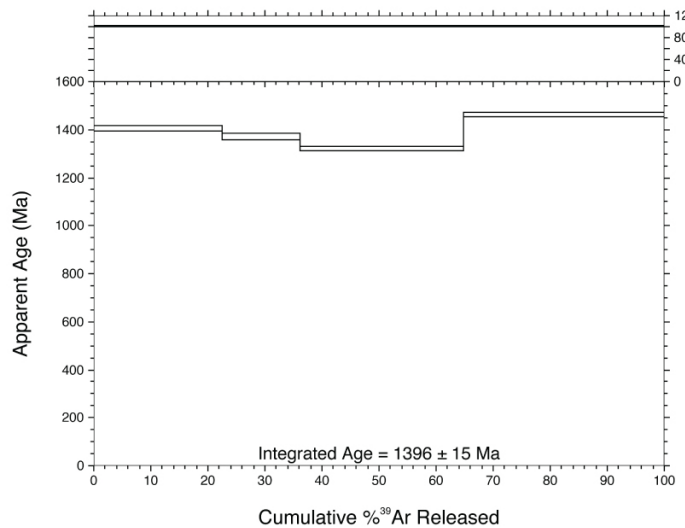
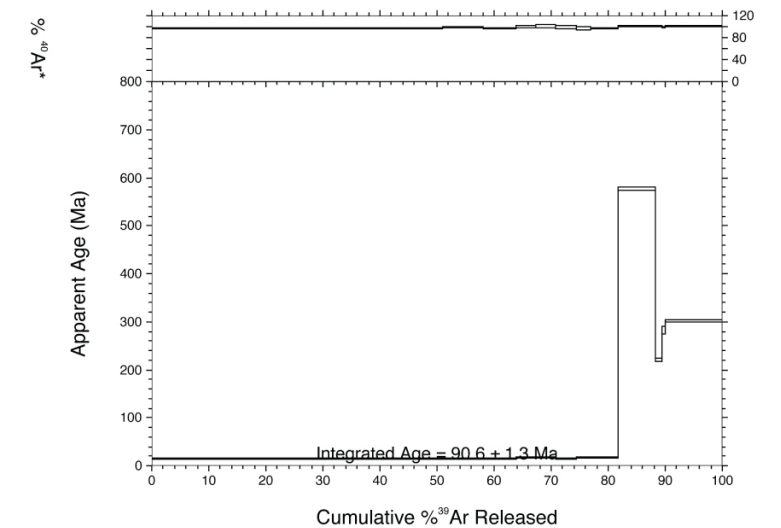
369 Corrie, S.L., M.J. Kohn, N. McQuarrie, and S.P. Long (2012), Flattening the Bhutan Himalaya:
370 *Earth and Plan. Sci. Lett.*, 349-350, 67-74, doi:10.1016/j.epsl.2012.07.001.

- 371
- 372 Daniel, C. G., L. S. Hollister, R. R. Parrish, and D. Grujic (2003), Exhumation of the Main
373 Central Thrust from lower crustal depths, eastern Bhutan Himalaya, *J. Metamorph. Geol.*, 21,
374 317–334, doi:10.1046/j.1525-1314.2003.00445.x.
- 375
- 376 Dumitru, T.A. (1993), A new computer-automated microscope stage system for fission-track
377 Analysis, *Nuclear Tracks and Radiation Measurements*, 21, 575-580.
- 378 Ehlers, T. A., T. Chaudhri, S. Kumar, C.W. Fuller, S.D. Willett, R.A. Ketcham, M.T. Brandon,
379 D.X. Belton, B.P. Kohn, A.J.W. Gleadow, T.J. Dunai, and F.Q. Fu (2005), Computational tools
380 for low-temperature thermochronometer interpretation, *Rev. Mineral. Geochem.*, 58, 589–622,
381 doi:10.2138/rmg.2005.58.22.
- 382
- 383 Gallagher, K., R. Brown, and C. Johnson (1998), Fission track analysis and its applications to
384 geological problems, *Ann. Rev. Earth Plan. Sci.* 26, 519-572.
- 385
- 386 Gehrels, G., V. Valencia, and A. Pullen (2006), Detrital zircon geochronology by laser
387 ablation multicollector ICPMS at the Arizona LaserChron Center, in T. Olszewski, ed.,
388 *Geochronology: Emerging Opportunities: Paleontology Society Papers*, 12, 67-76.
- 389
- 390 Gehrels, G.E., V. Valencia, and J. Ruiz (2008), Enhanced precision, accuracy, efficiency, and
391 spatial resolution of U-Pb ages by laser ablation multicollector inductively coupled plasma mass
392 spectrometry: *Geochem., Geophys., Geosystems*, 9, Q03017, doi:10.1029/2007GC001805.
- 393 Grujic, D., I. Coutand, B. Bookhagen, S. Bonnet, A. Blythe, and C. Duncan (2006), Climatic
394 forcing of erosion, landscape, and tectonics in the Bhutan Himalayas, *Geology*, 34, 801-804, doi:
395 10.1130/G22648.1.
- 396
- 397 Herman, F., P. Copeland, J.-P. Avouac, L. Bollinger, G. Maheo, P. LeFort, S. Rai, D. Foster, A.
398 Pecher, K. Stuwe, and P. Henry (2010), Exhumation, crustal deformation, and thermal structure
399 of the Nepal Himalaya derived from the inversion of thermochronological and thermobarometric
400 data and modeling of the topography, *J. Geophys. Res.*, 115, B0647, doi:10.1029/2008JB006126

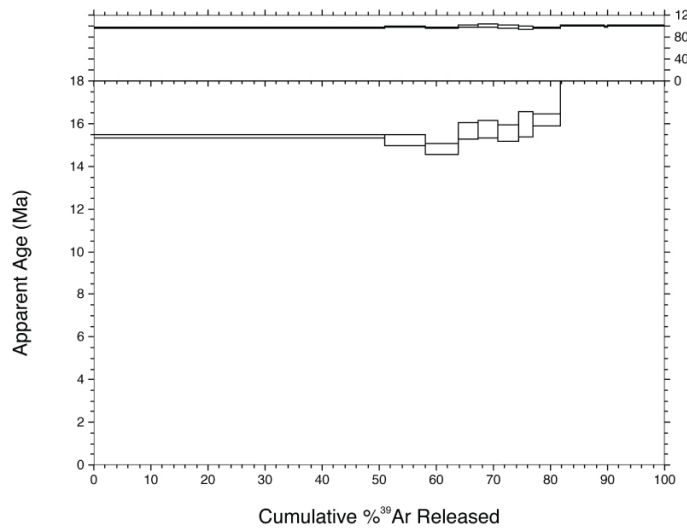
- 401
- 402 Hourigan, J.K., P.W. Reiners, and M.T. Brandon (2005), U-Th zonation-dependent alpha-
403 ejection in (U-Th)/He chronometry, *Geochimica et Cosmochimica Acta*, 69, 3349-3365.
- 404
- 405 Hurford, A.J. (1990), Standardization of fission-track dating calibration: recommendation
406 by the Fission Track Working Group of the I.U.G.S. Subcommission on Geochronology, *Chem.*
407 *Geol.* 80, 171-178.
- 408
- 409 Hurford, A.J., and P.F. Green (1983), The zeta age calibration of fission track dating, *Iosot.*
410 *Geosci.* 1, 285-317.
- 411
- 412 Kellett, D. A., D. Grujic, and S. Erdmann (2009), Miocene structural reorganization of the South
413 Tibetan detachment, eastern Himalaya: Implications for continental collision, *Lithosphere*, 1,
414 259–281, doi:10.1130/L56.1.
- 415
- 416 Kellett, D. A., D. Grujic, C. J. Warren, J. Cottle, R. A. Jamieson, and T. Tenzin (2010),
417 Metamorphic history of a syn-convergent orogen-parallel detachment: The South Tibetan
418 detachment system, Bhutan Himalaya, *J. Metamorph. Geol.*, 28, 785–808,
419 doi:10.1111/j.1525-1314.2010.00893.x.
- 420
- 421 Long, S., N. McQuarrie, T. Tobgay, and J. Hawthorne (2011c), Quantifying internal strain and
422 deformation temperature in the eastern Himalaya, Bhutan: Implications for the evolution of
423 strain in thrust sheets: *J. Struc. Geol.*, 22, 579-608, doi:10.1016/j.jsg.2010.12.011.
- 424
- 425 Ludwig, K.J. (2003), Isoplot 3.00: Berkeley Geochronology Center Special Publication 4, 70 p.
- 426
- 427 Miller, D.S., I.R. Duddy, P.F. Green, A.J. Hurford, and C.W. Naeser (1985), Results of
428 interlaboratory comparison of fission track age standards, Fission Track Workshop, 1984, *Nucl.*
429 *Tracks* 10, 383-391.

- 430 Ray, L., A. Bhattacharya, and S. Roy (2007), Thermal conductivity of Higher Himalayan
431 Crystallines from Garhwal Himalaya, India, *Tectonophysics*, 434, 71–79,
432 doi:10.1016/j.tecto.2007.02.003.
- 433
- 434 Reiners, P.W. (2005), Zircon (U-Th)/He thermochronometry: *Rev. in Min. and Geochem.*, 58,
435 151-179, doi:10.2138/rmg.2005.58.6.
- 436
- 437 Reiners, P.W., T.L. Spell, S. Nicolescu, and K.A. Zanetti (2004), Zircon (U-Th)/He
438 thermochronometry: He diffusion and comparisons with $^{40}\text{Ar}/^{39}\text{Ar}$ dating, *Geochim. et*
439 *Cosmochim. Acta*, 68, 1857-1887.
- 440
- 441 Reiners, P. W., and M. T. Brandon (2006), Using thermochronology to understand orogenic
442 erosion, *Ann. Rev. Earth Planet. Sci.*, 34, 419–466, doi:
443 10.1146/annurev.earth.34.031405.125202.
- 444
- 445 Schmitz, M.D., and S.A. Bowring (2001), U-Pb zircon and titanite systematics of the Fish
446 Canyon Tuff: an assessment of high-precision U-Pb geochronology and its application to young
447 volcanic rocks, *Geochimica et Cosmochimica Acta*, 65, 2571-2587, doi:10.1016/S0016-
448 7037(01)00616-0.
- 449 Schwarz, W. H. and M. Trieloff (2007), Intercalibration of $^{40}\text{Ar}-^{39}\text{Ar}$ age standards NL-25,
450 HB3gr hornblende, GA1550, SB-3, HD-B1 biotite and BMus/2 muscovite, *Chem. Geol.*, 242,
451 218-231.
- 452 Stacey, J.S., and J.D. Kramers (1975), Approximation of terrestrial lead isotope evolution by a
453 two-stage model: *Earth and Plan. Sci. Lett.*, 26, 207-221.
- 454 Steiger, R. H. and E. Jäger (1977), Subcommission on geochronology: Convention on the use of
455 decay constants in geo- and cosmochronology, *Earth Planet. Sci. Lett.*, 36, 21-23.
- 456

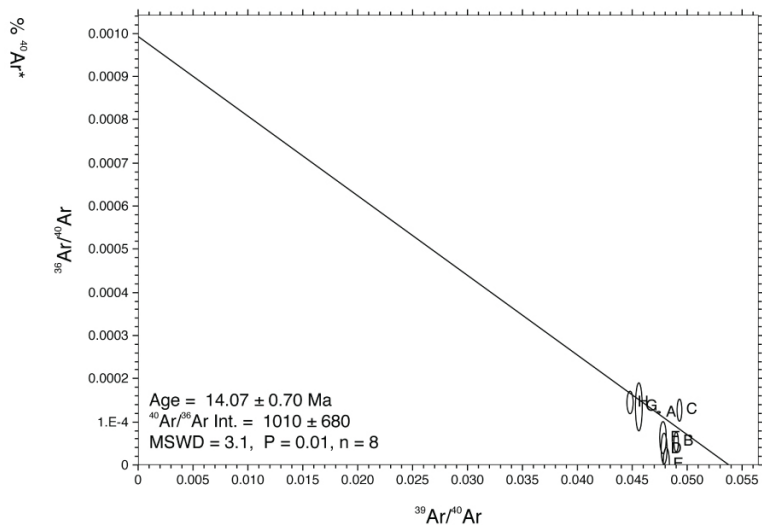
- 457 Stipp, M., H. Stunitz, R. Heilbronner, and S.M. Schmid, S.M. (2002), The eastern Tonale fault
458 zone: a ‘natural laboratory’ for crystal plastic deformation over a temperature range from 250° to
459 700°C, *J. Struct. Geol.*, 24, 1861-1884.
- 460
- 461 Stüwe, K., and D. Foster (2001), 40Ar/39Ar, pressure, temperature and fission track constraints
462 on the age and nature of metamorphism around the Main Central Thrust in the eastern Bhutan
463 Himalaya, *J. Asian Earth Sci.*, 19, 85–95, doi:10.1016/S1367-9120(00)00018-3.
- 464
- 465 Thiede, R.C., T.A. Ehlers, B. Bookhagen, and M.R. Strecker (2009), Erosional variability along
466 the northwest Himalaya, *Tectonics*, 114, F01015, doi:10.1029/2008JF001010.
- 467 Whipp, D. M., T.A. Ehlers, A.E. Blythe, K.W. Huntington, K.V. Hodges, and D.W. Burbank
468 (2007), Plio-Quaternary exhumation history of the central Nepalese Himalaya: 2.
469 Thermokinematic and thermochronometer age prediction model, *Tectonics*, 26, TC3003,
470 doi:10.1029/2006TC001991.
- 471 Whynot, N., D. Grujic, S. Long, and N. McQuarrie, N. (2010), Apparent temperature gradient
472 across the Lesser Himalayan Sequence: Raman spectroscopy on carbonaceous material in the
473 eastern Bhutan Himalaya, in M.L. Leech, S.L. Klemperer, and W.D. Mooney (eds.), Proceedings
474 for the 25th Himalaya-Karakoram Tibet Workshop, San Francisco, California, U.S.A.: U.S.
475 Geological Survey, Open-File Report 2010-1099, 2 p., <http://pubs.usgs.gov/of/2010-1099/whynot/>

A. BU07-9 spectrum**B. BU07-9 isochron****C. BU07-11 spectrum****D. BU07-11 isochron****E. BU07-21 spectrum****F. BU07-22 spectrum (all steps)**

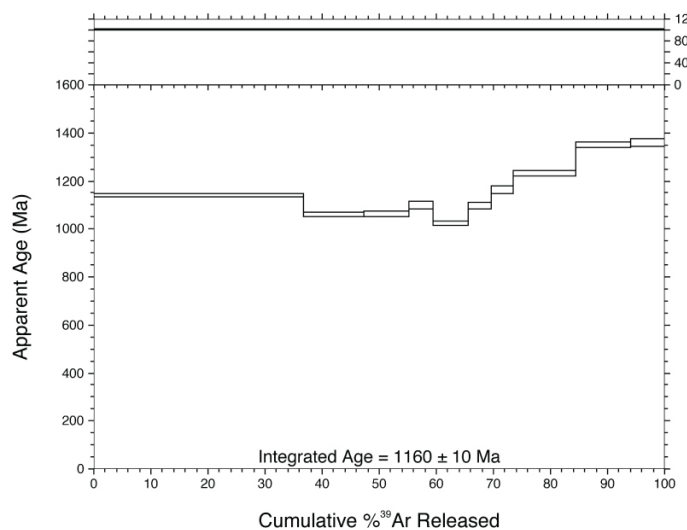
G. BU07-22 spectrum (low-temperature steps)



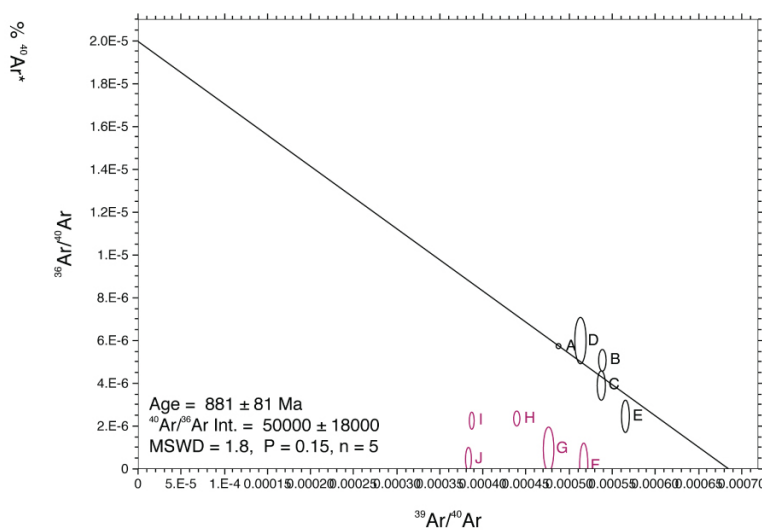
H. BU07-22 isochron (low-temperature steps)



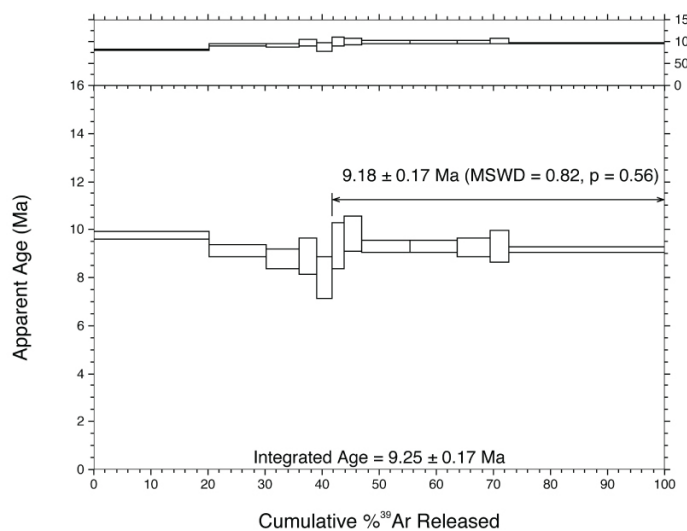
I. BU07-29 spectrum



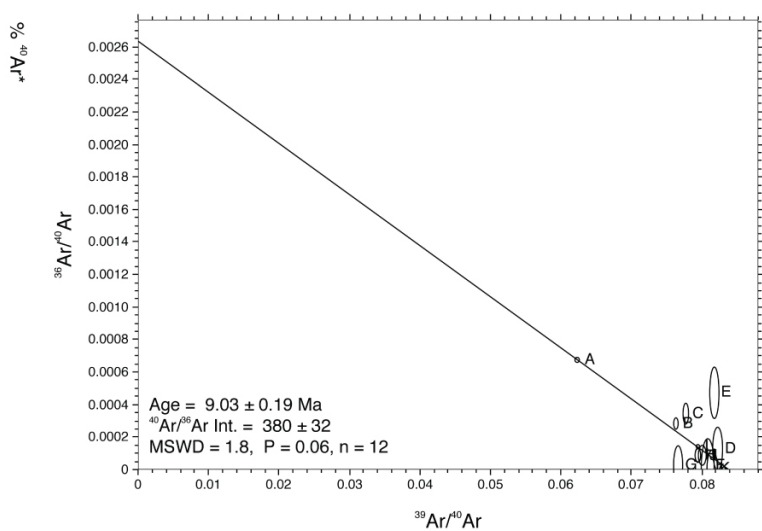
J. BU07-29 isochron (age from steps A-E shown)

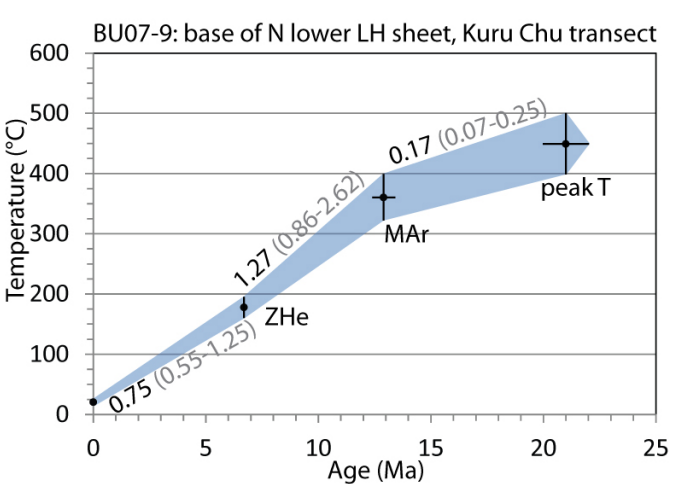
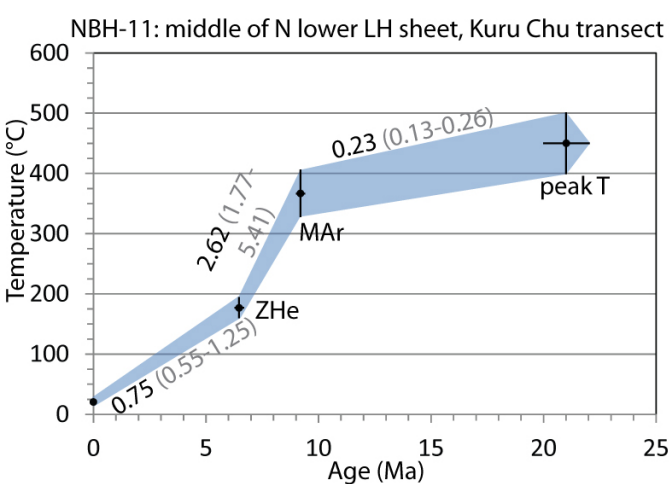
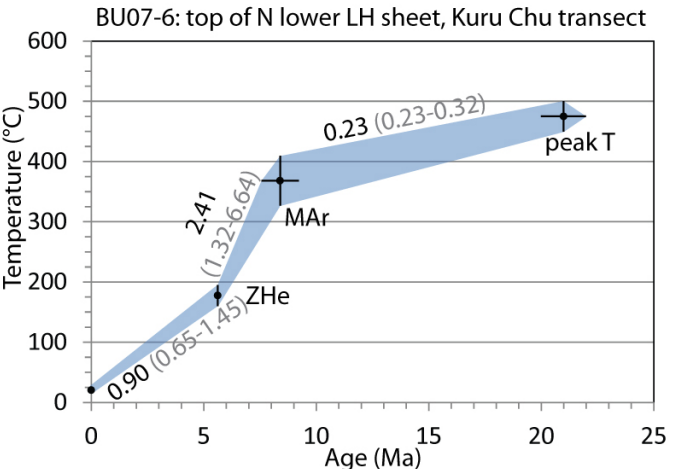
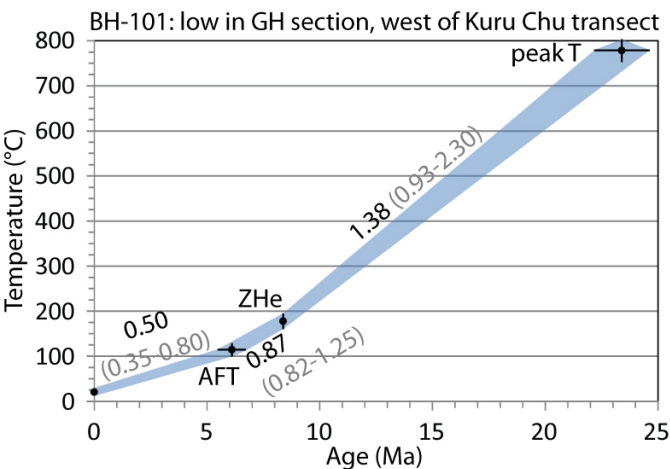
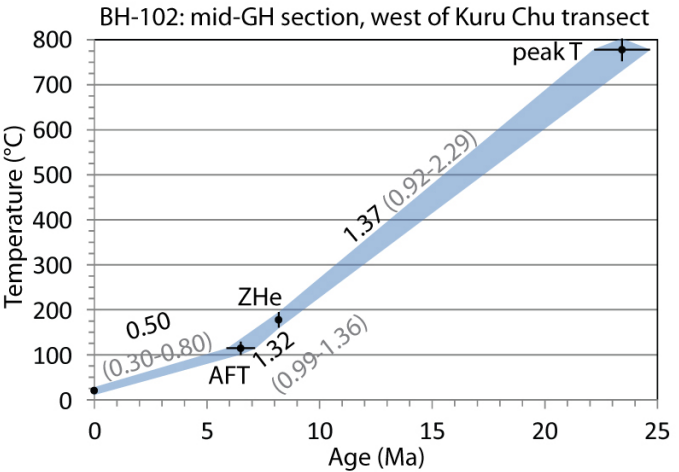
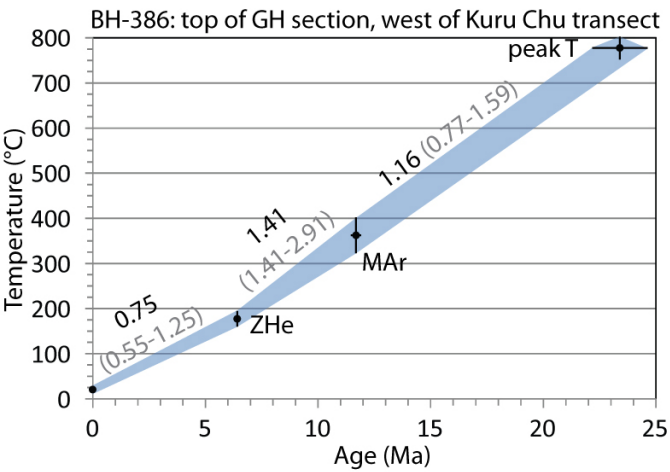
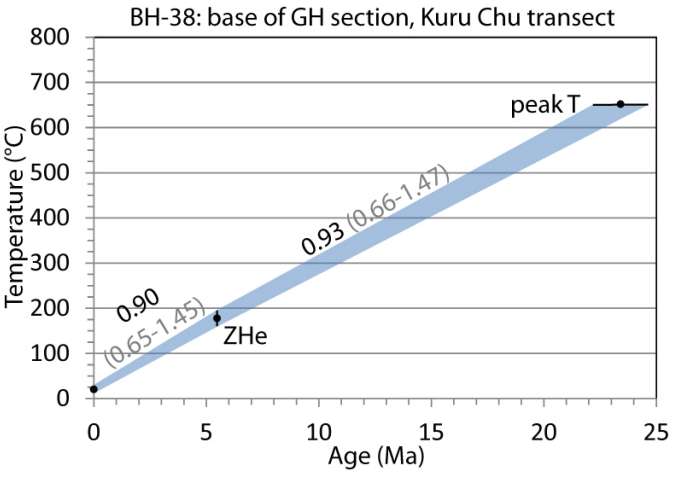
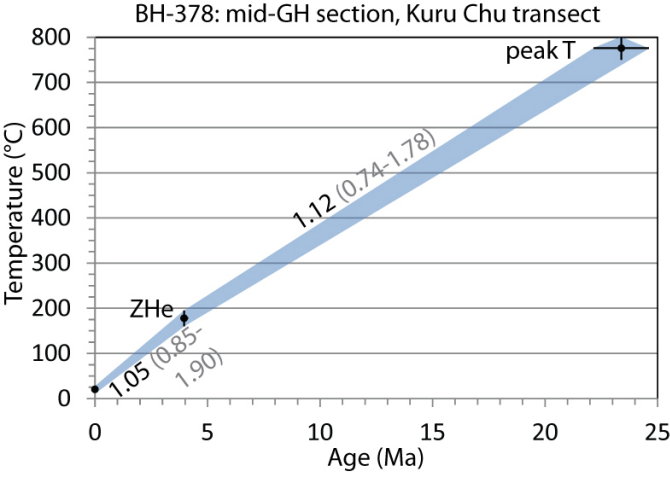


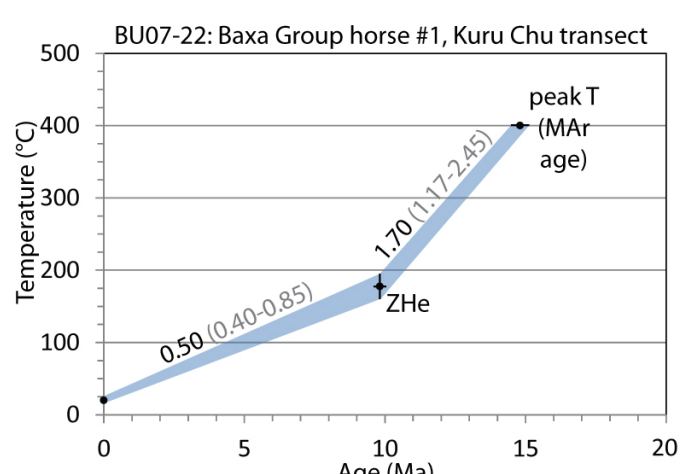
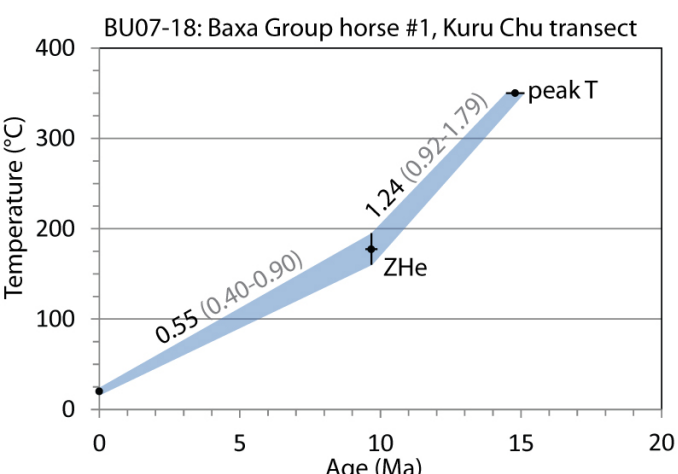
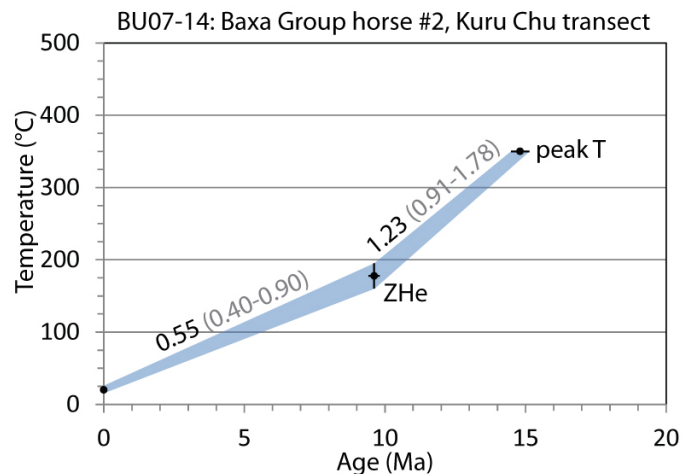
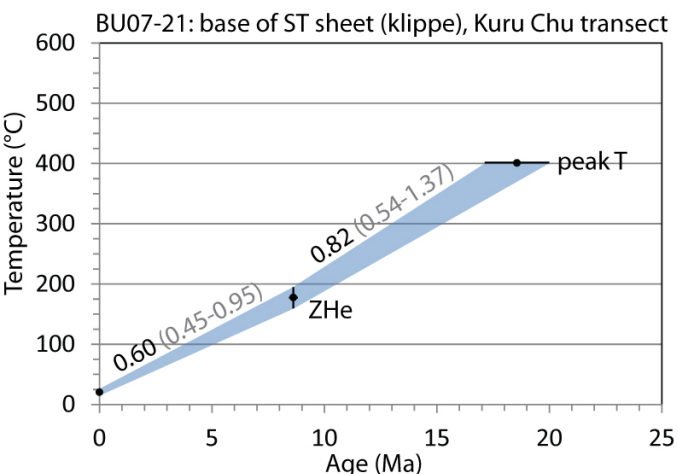
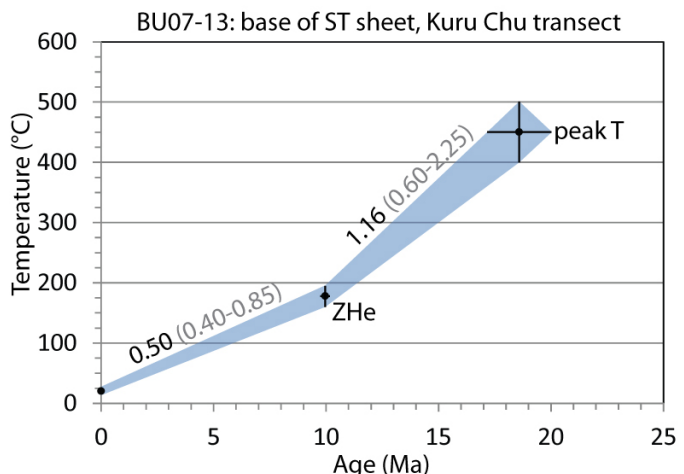
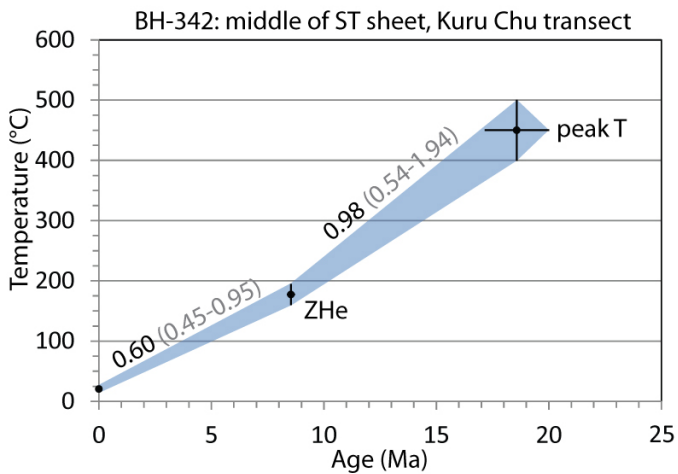
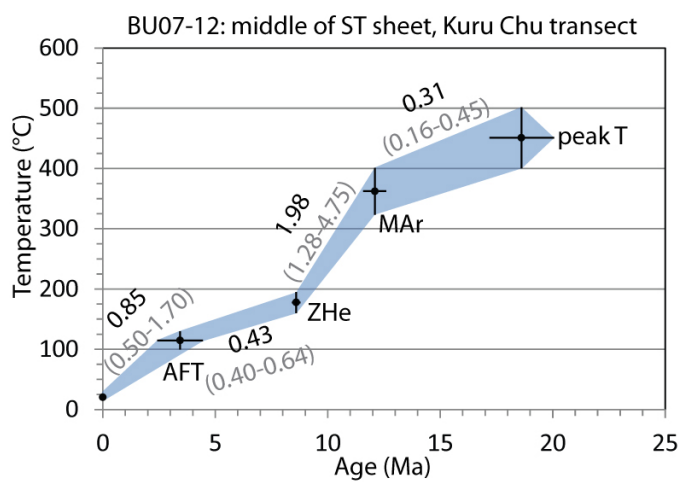
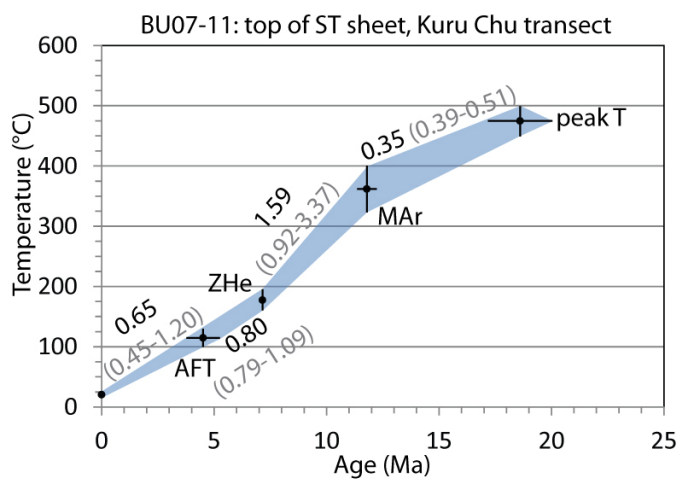
K. NBH-11 spectrum

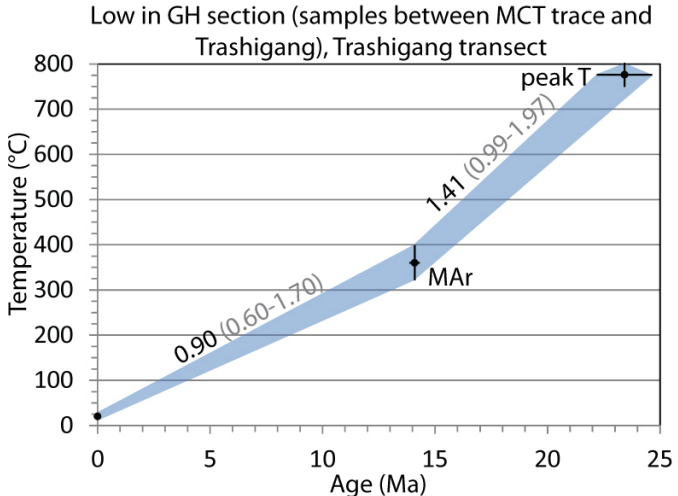
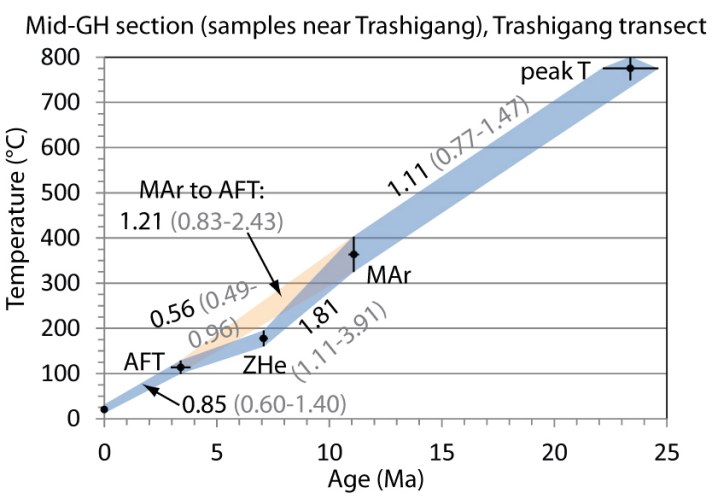
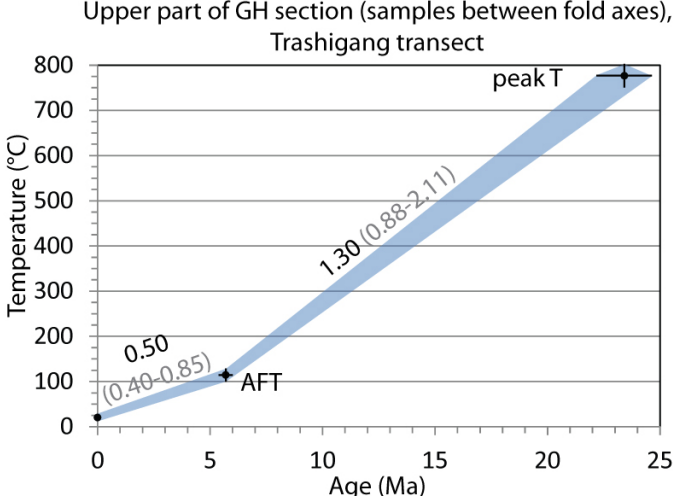
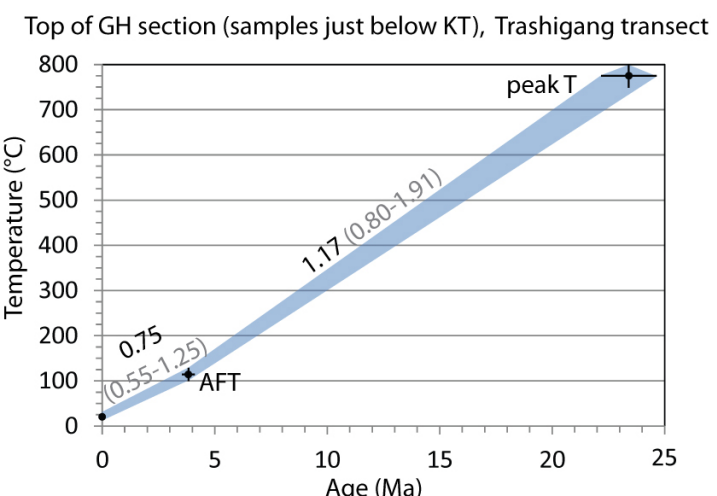
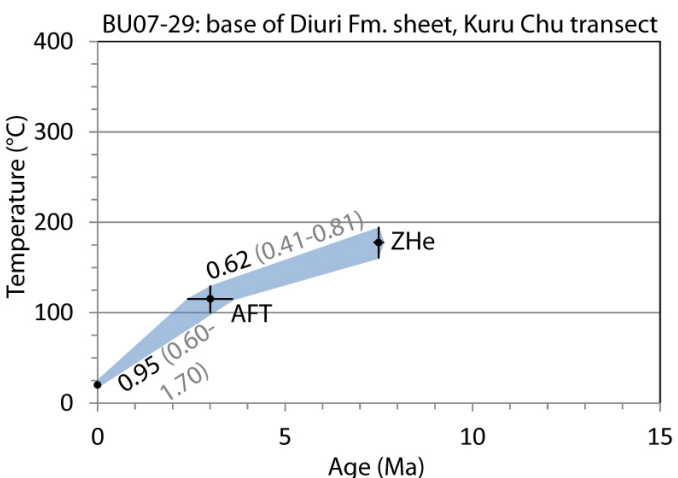
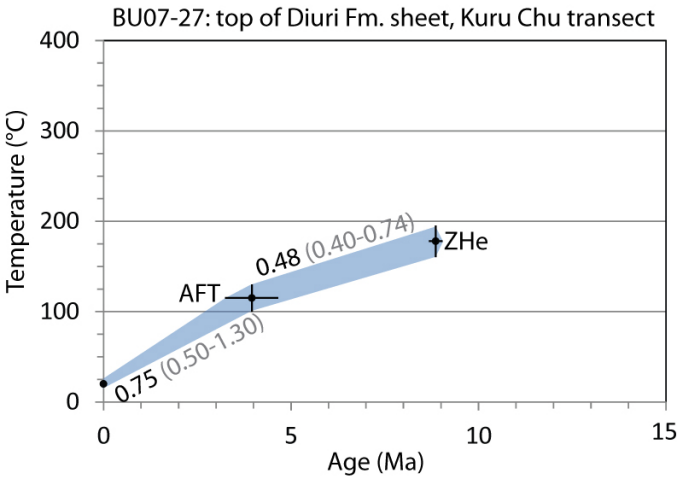
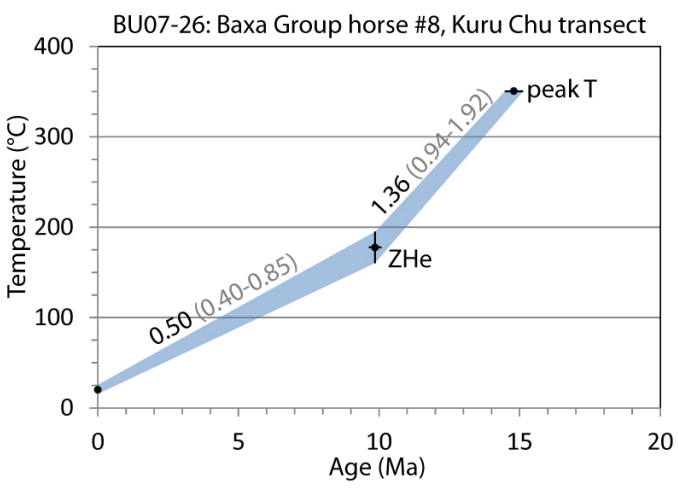
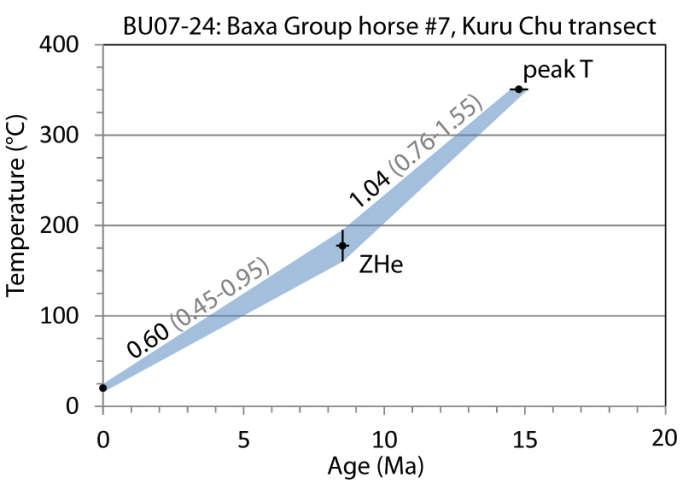


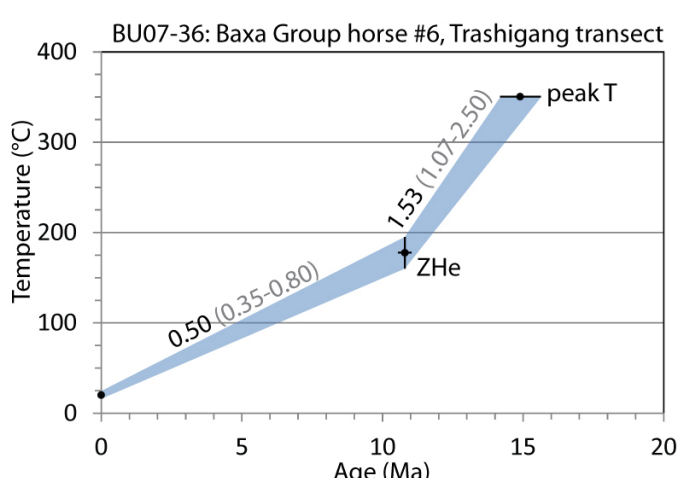
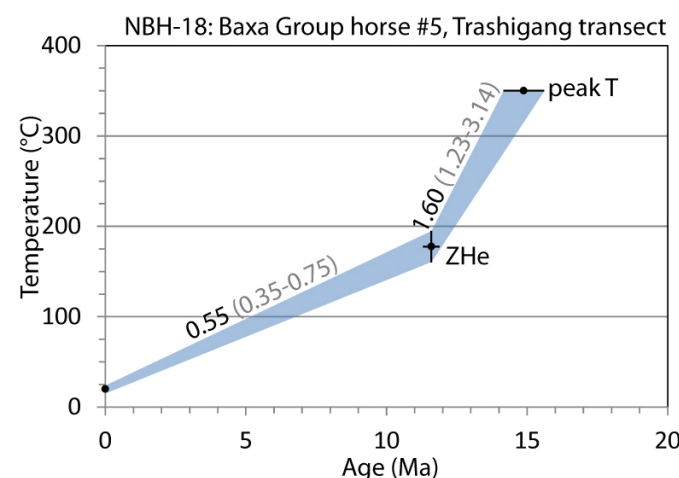
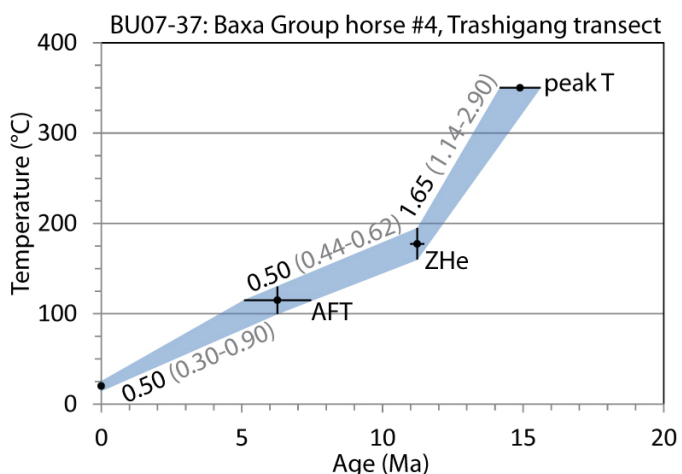
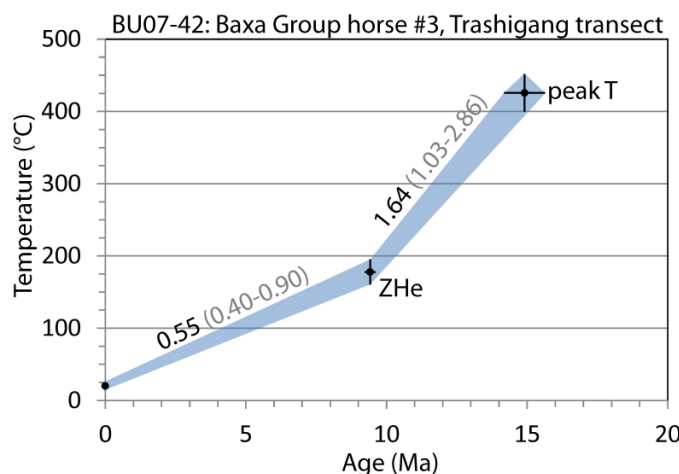
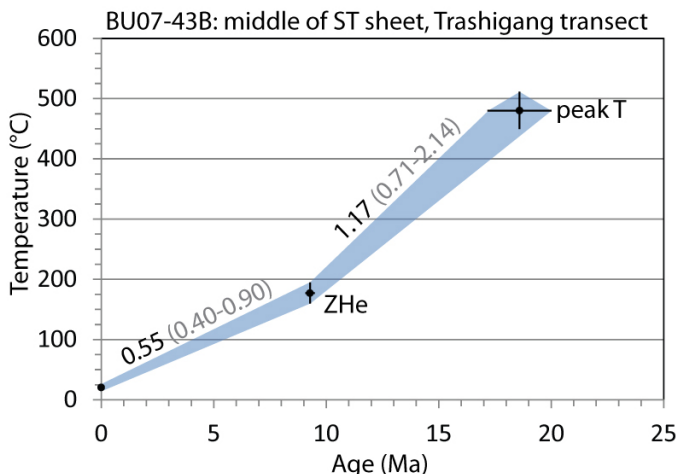
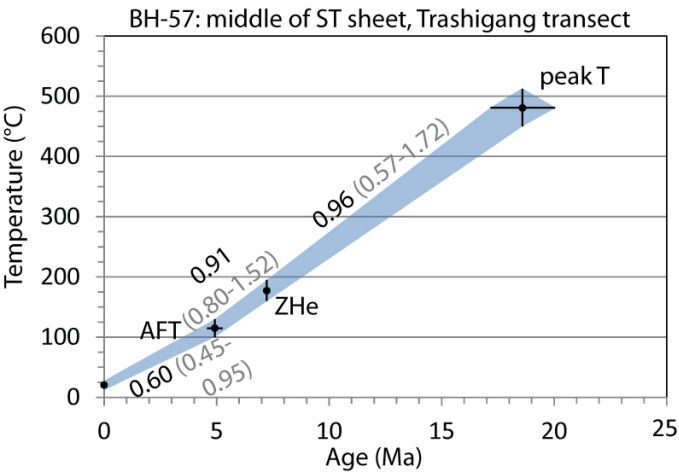
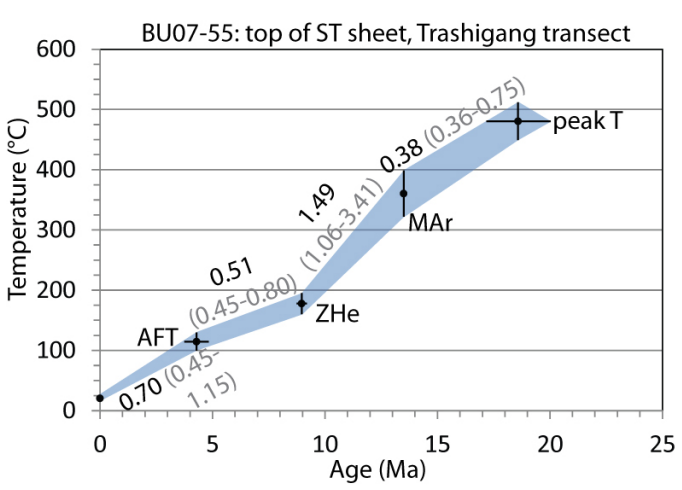
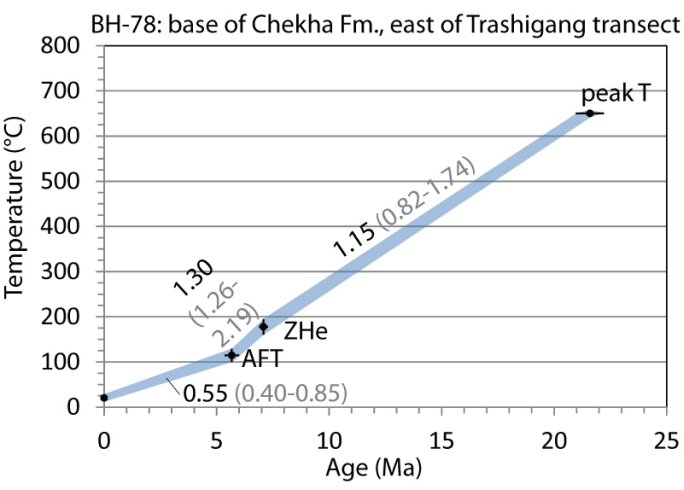
L. NBH-11 isochron











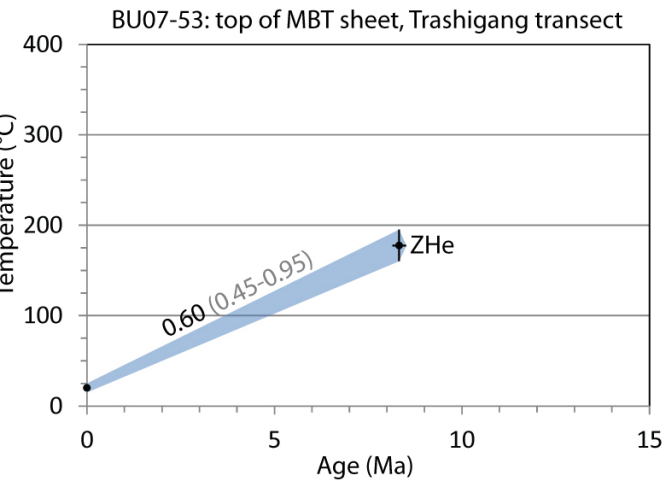
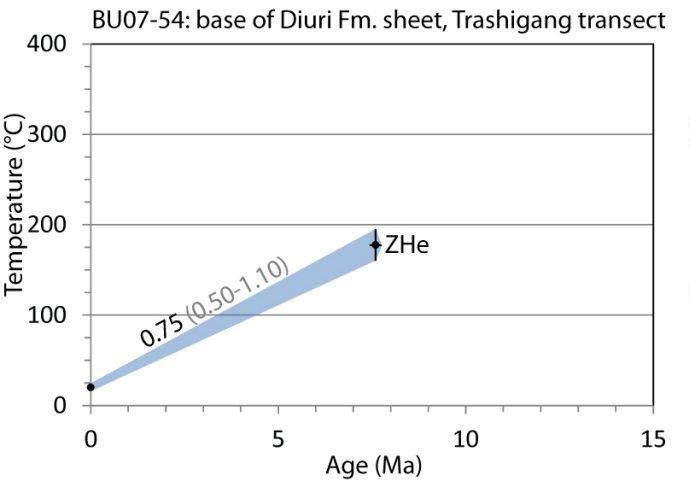
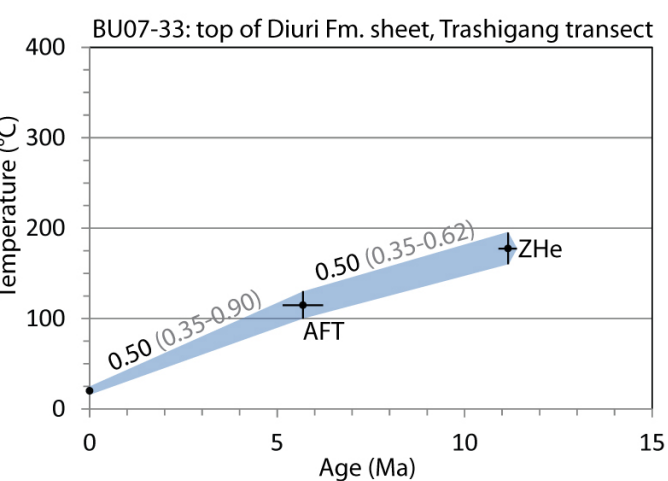
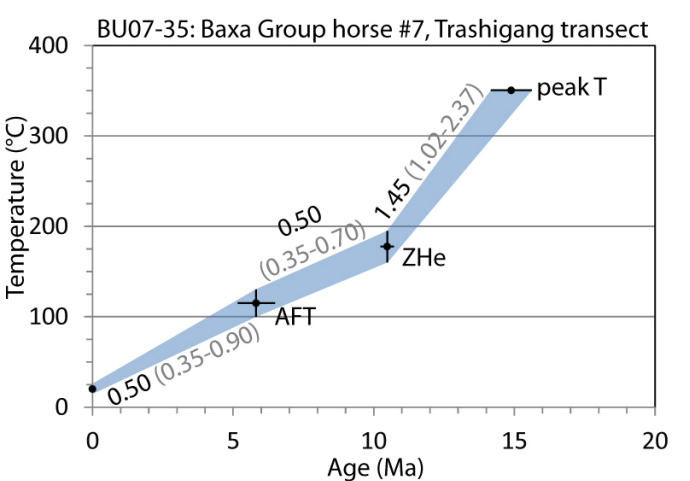


Table S1: white mica $^{40}\text{Ar}/^{39}\text{Ar}$ data

Lab ID#	Laser (W)	$^{40}\text{Ar}^*/^{39}\text{Ar}$ $\pm 2\sigma$		$^{40}\text{Ar}/^{39}\text{Ar}$ $\pm 2\sigma$		$^{38}\text{Ar}/^{39}\text{Ar}$ $\pm 2\sigma$		$^{36}\text{Ar}/^{39}\text{Ar}$ $\pm 2\sigma$		Cl/K	^{39}Ar (moles)	% $^{40}\text{Ar}^*$	% ^{39}Ar	Age (Ma) $\pm 2\sigma$	J value	J value error (2σ)
Sample	BU07-6														4.2260E-04	7.2206E-06
354-01A	5.9	12.310	1.429	15.865	0.318	0.0156	0.0046	0.0119	0.0048	0.002	1.46E-17	77.73	35.79	9.36	1.08	
354-01B	15.0	10.343	1.074	16.427	0.253	0.0178	0.0026	0.0205	0.0036	0.002	2.62E-17	63.07	64.21	7.87	0.82	
Sample	BU07-9														4.1910E-04	1.1041E-05
391-01A	5.4	17.812	0.409	19.607	0.178	0.0147	0.0014	0.0060	0.0013	0.002	7.36E-17	90.97	50.91	13.42	0.31	
391-01B	5.9	16.255	1.580	17.563	0.337	0.0125	0.0045	0.0043	0.0052	0.002	1.71E-17	92.70	11.85	12.25	1.19	
391-01C	9.0	15.730	1.580	15.870	0.346	0.0105	0.0049	0.0004	0.0052	0.002	1.70E-17	99.29	11.76	11.85	1.19	
391-01D	15.0	17.048	0.766	17.933	0.226	0.0156	0.0023	0.0029	0.0025	0.003	3.68E-17	95.21	25.48	12.84	0.58	
Sample	BU07-11														4.1020E-04	1.1333E-05
387-01A	5.0	16.869	0.404	20.200	0.168	0.0146	0.0012	0.0112	0.0013	0.002	7.93E-17	83.62	34.54	12.44	0.30	
387-01B	5.4	16.004	1.057	17.307	0.273	0.0110	0.0031	0.0043	0.0035	0.002	2.58E-17	92.62	11.25	11.80	0.78	
387-01C	5.7	13.155	3.162	18.620	0.716	0.0143	0.0082	0.0184	0.0106	0.002	8.51E-18	70.76	3.70	9.71	2.33	
387-01D	6.2	12.337	2.735	12.458	0.391	0.0145	0.0068	0.0003	0.0092	0.002	1.08E-17	99.25	4.68	9.11	2.01	
387-01E	9.0	15.479	0.706	15.537	0.192	0.0132	0.0019	0.0001	0.0023	0.002	4.49E-17	99.81	19.57	11.42	0.52	
387-01F*	9.3	0.957	5.589	1.709	0.402	0.0116	0.0132	0.0025	0.0189	0.002	5.30E-18	56.90	2.31	0.71	4.13	
387-01G	15.0	16.236	0.523	17.140	0.183	0.0132	0.0016	0.0030	0.0017	0.002	5.50E-17	94.88	23.94	11.97	0.38	
*Step F was excluded from the age spectrum (insufficient ^{40}Ar content).																
Sample	BU07-12														4.3290E-04	1.1121E-05
389-01A	5.9	16.102	0.796	18.203	0.253	0.0156	0.0020	0.0070	0.0026	0.002	3.20E-17	88.60	32.26	12.53	0.62	
389-01B	15.0	15.294	0.344	16.745	0.132	0.0140	0.0012	0.0048	0.0011	0.002	6.72E-17	91.49	67.74	11.90	0.27	
Sample	BU07-21														4.0950E-04	5.7258E-06
356-03A	5.4	2871.541	32.491	2872.356	32.495	0.0138	0.0019	0.0027	0.0018	0.002	4.08E-17	99.97	22.65	1402.59	11.03	
356-03B	5.9	2771.964	38.748	2772.959	38.752	0.0111	0.0025	0.0033	0.0029	0.002	2.45E-17	99.97	13.59	1368.46	13.41	
356-03C	9.0	2633.066	27.204	2633.840	27.207	0.0132	0.0016	0.0025	0.0016	0.002	5.16E-17	99.97	28.60	1319.74	9.67	
356-03D	15.0	3046.011	26.754	3046.564	26.755	0.0117	0.0013	0.0018	0.0015	0.002	6.34E-17	99.98	35.16	1460.87	8.80	
Sample	BU07-22														4.2120E-04	6.05E-06
394-01B	5.2	20.086	0.310	20.435	0.144	0.0134	0.0011	0.0011	0.0009	0.002	9.13E-17	98.43	14.42	15.20	0.23	
394-01C	5.4	19.528	0.348	20.318	0.167	0.0124	0.0011	0.0026	0.0010	0.002	7.46E-17	96.25	11.78	14.78	0.26	
394-01D	5.5	20.666	0.523	20.915	0.233	0.0135	0.0017	0.0008	0.0016	0.002	4.65E-17	98.94	7.34	15.64	0.39	
394-01E	5.7	20.791	0.539	20.821	0.228	0.0119	0.0016	0.0000	0.0017	0.002	4.45E-17	99.99	7.03	15.73	0.41	
394-01F	5.9	20.520	0.518	20.928	0.195	0.0105	0.0015	0.0013	0.0016	0.002	4.64E-17	98.18	7.32	15.53	0.39	
394-01G	6.2	21.060	0.771	21.958	0.271	0.0133	0.0021	0.0030	0.0025	0.002	3.29E-17	96.03	5.20	15.93	0.58	
394-01H	7.8	21.345	0.405	22.319	0.192	0.0142	0.0014	0.0032	0.0012	0.002	6.31E-17	95.76	9.95	16.15	0.31	
394-01I	9.0	892.900	8.161	893.981	8.164	0.0137	0.0011	0.0036	0.0010	0.002	8.23E-17	99.88	12.99	575.96	4.51	
394-01J	9.1	307.622	5.655	309.019	5.497	0.0135	0.0040	0.0046	0.0048	0.002	1.54E-17	99.56	2.43	219.81	3.80	
394-01K	9.3	398.965	12.167	404.094	11.894	0.0137	0.0086	0.0173	0.0108	0.002	7.58E-18	98.74	1.20	280.23	7.92	
394-01L	15.0	430.201	2.917	431.131	2.914	0.0126	0.0009	0.0031	0.0007	0.002	1.29E-16	99.79	20.34	300.44	1.88	
Sample	BU07-29														4.3100E-04	4.74E-06
396-01A	5.0	2044.362	16.694	2047.833	16.704	0.0152	0.0008	0.0117	0.0007	0.002	1.42E-16	99.83	36.74	1139.96	6.90	
396-01B	5.2	1850.261	21.298	1853.061	21.313	0.0143	0.0016	0.0094	0.0019	0.002	4.13E-17	99.85	10.67	1057.89	9.21	
396-01C	5.4	1856.351	27.101	1858.516	27.116	0.0136	0.0023	0.0072	0.0025	0.002	3.04E-17	99.88	7.85	1060.52	11.71	
396-01D	5.5	1942.298	42.749	1945.746	42.799	0.0161	0.0038	0.0116	0.0044	0.002	1.61E-17	99.82	4.17	1097.27	18.09	
396-01E	5.7	1765.652	23.535	1766.948	23.534	0.0141	0.0025	0.0043	0.0028	0.002	2.44E-17	99.93	6.32	1020.91	10.39	
396-01F	5.9	1933.997	33.934	1934.090	33.912	0.0118	0.0039	0.0002	0.0042	0.002	1.56E-17	100.00	4.02	1093.75	14.39	
396-01G	6.2	2094.332	42.635	2094.928	42.626	0.0118	0.0036	0.0019	0.0043	0.002	1.46E-17	99.97	3.77	1160.50	17.42	
396-01H	7.8	2270.214	26.626	2271.803	26.635	0.0117	0.0018	0.0053	0.0017	0.002	4.28E-17	99.93	11.07	1230.98	10.46	
396-01I	9.0	2580.625	33.663	2582.368	33.675	0.0123	0.0019	0.0058	0.0021	0.002	3.69E-17	99.93	9.53	1349.03	12.39	
396-01J	9.3	2608.882	44.949	2609.248	44.946	0.0138	0.0025	0.0012	0.0029	0.002	2.27E-17	99.99	5.87	1359.40	16.45	
Sample	NBH-11														4.2080E-04	6.4858E-06
392-01A	5.0	12.845	0.210	16.042	0.093	0.0145	0.0006	0.0107	0.0007	0.002	1.87E-16	80.21	20.32	9.72	0.16	
392-01B	5.2	12.021	0.325	13.124	0.099	0.0133	0.0011	0.0036	0.0011	0.002	9.11E-17	91.79	9.92	9.10	0.25	
392-01C	5.2	11.575	0.539	12.891	0.127	0.0124	0.0016	0.0044	0.0018	0.002	5.31E-17	89.99	5.77	8.76	0.41	
392-01D	5.5	11.701	0.999	12.170	0.176	0.0153	0.0026	0.0015	0.0033	0.003	2.83E-17	96.36	3.09	8.86	0.75	
392-01E	5.7	10.525	1.163	12.254	0.193	0.0139	0.0028	0.0058	0.0039	0.002	2.42E-17	86.08	2.64	7.97	0.88	
392-01F	5.9	12.272	1.258	12.374	0.232	0.0140	0.0038	0.0003	0.0042	0.002	2.05E-17	99.41	2.23	9.29	0.95	
392-01G	6.2	12.943	0.965	13.059	0.185	0.0117	0.0028	0.0003	0.0032	0.002	2.73E-17	99.32	2.97	9.80	0.73	
392-01H	7.8	12.263	0.346	12.601	0.100	0.0129	0.0011	0.0011	0.0011	0.002	7.79E-17	97.53	8.48	9.28	0.26	
392-01I	9.0	12.258	0.357	12.604	0.105	0.0133	0.0011	0.0011	0.0012	0.002	7.72E-17	97.47	8.41	9.28	0.27	
392-01J	9.1	12.172	0.517	12.498	0.134	0.0119	0.0016	0.0010	0.0017	0.002	5.17E-17	97.61	5.63	9.22	0.39	
392-01K	9.3	12.252	0.878	12.285	0.185	0.0128	0.0026	0.0000	0.0029	0.002	3.13E-17	99.97	3.41	9.28	0.66	
392-01L	15.0	12.069	0.134	12.608	0.060	0.0125	0.0006	0.0017	0.0004	0.002	2.49E-16	95.94	27.15	9.14	0.10	

Table S2: Single grain zircon (U-Th)/He ages and supporting data

Sample name	ng U	ng Th	Raw age (Ma)	Est 2σ error	Mass (μg)	half-width (μm)	U (ppm)	Th (ppm)	Th/U	⁴ He (nmol/g)	^a Ft	Corrected age (Ma)	Est 2σ error
BH-38_z1	1.66	0.08	3.81	0.12		44.25	660	30	0.05	0.03	0.73	5.23	0.17
BH-38_z2	2.50	0.23	4.14	0.13		41.75	1156	105	0.09	0.06	0.71	5.80	0.18
weighted mean												5.49	0.12
BH-57_z1	1.42	0.47	5.13	0.14		50.50	343	115	0.33	0.04	0.76	6.76	0.18
BH-57_z2	0.50	0.36	5.36	0.15		42.50	189	137	0.72	0.02	0.71	7.51	0.21
BH-57_z3	2.42	0.90	5.54	0.15		44.25	715	266	0.37	0.08	0.73	7.63	0.21
weighted mean												7.26	0.11
BH-78_z2	0.54	0.19	5.00	0.15		43.00	209	75	0.36	0.02	0.72	6.95	0.20
BH-78_z3	3.71	0.48	5.01	0.14		38.75	1998	258	0.13	0.10	0.69	7.23	0.21
weighted mean												7.09	0.14
BH-101_z1	20.67	8.44	7.32	0.20		92.67	738	302	0.41	31.83	0.86	8.48	0.23
BH-101_z2	9.17	5.69	6.08	0.17		50.98	1730	1074	0.62	64.85	0.76	8.02	0.23
BH-101_z3	35.34	11.05	7.09	0.19		69.34	2882	901	0.31	117.86	0.82	8.64	0.23
weighted mean												8.37	0.13
BH-102_z1	19.20	0.64	6.37	0.19		56.99	1529	51	0.03	52.72	0.79	8.11	0.24
BH-102_z2	68.54	2.79	7.15	0.21		94.33	1589	65	0.04	61.60	0.87	8.24	0.25
BH-102_z3	20.25	0.63	6.75	0.20		70.04	1216	38	0.03	44.45	0.82	8.20	0.25
weighted mean												8.18	0.14
BH-342_z1	1.98	0.53	6.63	0.19		51.50	377	102	0.27	0.07	0.76	8.70	0.25
BH-342_z2	2.38	1.21	7.30	0.20		64.25	259	132	0.51	0.10	0.81	9.06	0.25
BH-342_z3	2.20	0.58	6.16	0.17		53.00	408	107	0.26	0.08	0.77	8.01	0.23
weighted mean												8.55	0.14
BH-378_z1	44.79	2.58	3.32	0.09		84.25	1997	115	0.06	0.81	0.85	3.90	0.11
BH-378_z2	18.34	0.90	3.97	0.11		59.25	2294	112	0.05	0.40	0.79	5.00	0.14
BH-378_z3	16.65	1.27	3.03	0.08		71.00	1245	95	0.08	0.28	0.83	3.67	0.10
weighted mean												4.05	0.07
BH-386_z1	1.38	0.52	5.60	0.16		62.21	172	65	0.38	5.63	0.80	7.00	0.19
BH-386_z2	1.02	0.35	5.01	0.15		47.94	258	89	0.34	7.52	0.75	6.71	0.20
BH-386_z3	0.62	0.27	4.21	0.13		45.64	181	80	0.44	4.52	0.73	5.74	0.17

weighted mean												6.42	0.11
BU07-6-z1	1.55	0.86	4.60	0.17	4.66	50.50	333	185	0.55	9.33	0.79	5.84	0.21
BU07-6-z2	1.34	0.12	4.37	0.17	3.41	45.50	394	36	0.09	9.46	0.77	5.68	0.22
BU07-6-z3	2.16	0.67	4.06	0.14	2.89	40.50	748	232	0.31	17.55	0.75	5.43	0.18
weighted mean												5.62	0.12
BU07-9-z1	2.04	0.88	5.28	0.19	5.20	45.25	393	169	0.43	12.32	0.78	6.80	0.24
BU07-9-z2	8.25	1.75	5.36	0.19	10.21	48.00	808	172	0.21	24.51	0.80	6.69	0.24
BU07-9-z3	1.11	0.59	5.51	0.18	9.81	62.75	113	61	0.54	3.78	0.83	6.64	0.21
weighted mean												6.70	0.13
BU07-11-z1	2.03	0.53	5.58	0.21	7.20	46.25	282	73	0.26	9.00	0.78	7.14	0.27
BU07-11-z2	2.21	0.50	7.13	0.27	7.25	52.50	305	69	0.23	12.34	0.80	8.93	0.34
BU07-11-z3	3.63	0.66	5.09	0.18	7.11	48.50	511	94	0.18	14.63	0.79	6.42	0.22
weighted mean												7.16	0.15
BU07-12-z1	8.90	3.49	7.71	0.39	21.23	83.50	419	164	0.39	19.05	0.87	8.87	0.44
BU07-12-z2	1.59	0.49	6.49	0.22	5.80	43.75	274	85	0.31	10.27	0.77	8.39	0.28
BU07-12-z3	1.13	1.37	7.34	0.21	15.19	70.25	74	90	1.22	3.79	0.85	8.68	0.25
weighted mean												8.60	0.17
BU07-13-z1	0.52	0.19	8.33	0.29	1.85	38.25	278	102	0.37	13.58	0.72	11.52	0.40
BU07-13-z2	0.49	0.49	8.87	0.29	1.96	38.75	250	251	1.00	14.81	0.72	12.27	0.40
BU07-13-z3	0.99	0.50	5.92	0.20	1.89	41.00	524	263	0.50	18.72	0.73	8.11	0.28
weighted mean												9.97	0.20
BU07-14-z1	2.78	1.47	7.75	0.25	7.35	58.50	378	200	0.53	17.78	0.82	9.51	0.30
BU07-14-z2	2.88	4.15	7.38	0.21	5.69	54.00	506	730	1.44	27.01	0.80	9.26	0.26
BU07-14-z3	3.78	2.43	7.97	0.25	3.89	48.25	971	623	0.64	48.07	0.78	10.27	0.32
weighted mean												9.62	0.17
BU07-18-z1	7.16	2.71	8.19	0.28	11.52	57.75	622	235	0.38	29.89	0.82	9.95	0.34
BU07-18-z2	2.91	1.48	8.32	0.27	15.76	80.50	184	94	0.51	9.27	0.86	9.69	0.32
BU07-18-z3	1.44	0.69	7.42	0.25	4.28	51.50	337	161	0.48	14.98	0.79	9.43	0.32
weighted mean												9.68	0.19
BU07-21-z1	1.95	1.73	7.59	0.24	8.23	55.75	237	210	0.89	11.73	0.81	9.36	0.30
BU07-21-z2	1.15	0.40	6.11	0.20	7.15	48.75	161	56	0.35	5.73	0.79	7.73	0.26
BU07-21-z3	3.69	1.04	7.19	0.24	7.52	46.50	490	139	0.28	20.26	0.79	9.12	0.30
weighted mean												8.62	0.16

BU07-22-z1	12.81	6.21	8.26	0.27	16.74	87.50	765	371	0.48	37.98	0.87	9.55	0.32
BU07-22-z2	18.73	5.36	8.65	0.30	29.21	95.00	641	184	0.29	31.90	0.88	9.79	0.34
BU07-22-z3	1.08	0.03	8.12	0.30	5.19	50.00	208	7	0.03	9.15	0.79	10.24	0.37
weighted mean												9.82	0.20
BU07-24-z1	0.37	0.33	7.35	0.25	2.10	40.75	178	158	0.89	8.55	0.73	10.04	0.35
BU07-24-z2	2.07	0.53	5.54	0.20	1.80	41.50	1147	292	0.25	36.32	0.73	7.59	0.27
weighted mean												8.52	0.21
BU07-26-z1	0.15	0.01	8.12	0.32	3.56	36.00	43	4	0.09	1.93	0.73	11.07	0.44
BU07-26-z2	1.41	0.82	7.86	0.25	4.60	44.75	307	178	0.58	14.81	0.77	10.26	0.32
BU07-26-z3	4.75	1.48	6.54	0.22	3.12	36.50	1523	473	0.31	57.66	0.73	8.95	0.30
weighted mean												9.86	0.20
BU07-27-z1	2.94	2.65	8.56	0.26	7.84	59.50	375	337	0.90	21.02	0.82	10.48	0.32
BU07-27-z2	6.32	3.62	6.16	0.20	5.71	51.50	1106	634	0.57	41.67	0.80	7.74	0.25
BU07-27-z3	2.06	0.56	6.92	0.23	4.35	44.00	472	128	0.27	18.72	0.76	9.06	0.31
weighted mean												8.86	0.16
BU07-29-z1	0.61	0.77	6.90	0.21	4.90	55.50	125	157	1.25	6.05	0.79	8.69	0.26
BU07-29-z2	1.43	0.87	6.70	0.21	4.25	42.00	338	206	0.61	13.95	0.76	8.86	0.28
BU07-29-z3	1.00	0.92	4.52	0.14	3.06	36.75	326	302	0.93	9.67	0.73	6.22	0.19
weighted mean												7.50	0.13
BU07-33-z1	2.59	0.31	8.10	0.31	5.81	41.75	446	53	0.12	20.02	0.77	10.55	0.41
BU07-33-z2	0.64	0.10	8.30	0.32	3.52	38.50	181	27	0.15	8.39	0.74	11.25	0.43
BU07-33-z3	1.42	1.01	8.95	0.28	4.00	47.00	354	252	0.71	19.97	0.77	11.57	0.36
weighted mean												11.16	0.23
BU07-35-z1	2.65	3.34	9.43	0.30	14.99	57.75	176	223	1.26	11.65	0.83	11.42	0.37
BU07-35-z2	11.11	3.72	10.57	0.39	26.19	96.00	424	142	0.33	26.08	0.88	11.99	0.44
BU07-35-z3	1.19	1.10	7.81	0.23	10.36	70.00	115	106	0.93	5.89	0.84	9.32	0.28
weighted mean												10.48	0.20
BU07-36-z1	2.60	2.31	9.74	0.34	8.39	64.00	310	275	0.89	19.71	0.83	11.80	0.41
BU07-36-z2	3.75	2.48	8.92	0.31	5.12	54.50	732	484	0.66	40.69	0.80	11.18	0.39
BU07-36-z3	2.81	2.55	8.45	0.25	11.24	72.50	250	227	0.91	13.83	0.84	10.03	0.30
weighted mean												10.80	0.21
BU07-37-z1	3.18	1.26	8.42	0.28	3.85	44.75	826	327	0.40	40.97	0.76	11.10	0.38

BU07-37-z2	3.72	3.02	9.00	0.29	6.81	60.75	547	444	0.81	31.60	0.82	11.04	0.36
BU07-37-z3	18.63	7.99	10.33	0.34	31.35	110.50	594	255	0.43	36.44	0.89	11.60	0.38
weighted mean												11.24	0.22
BU07-42-z1	0.51	0.92	7.36	0.23	2.45	41.75	207	373	1.80	11.74	0.74	9.98	0.31
BU07-42-z2	0.94	1.01	6.13	0.20	2.30	43.25	410	440	1.07	17.02	0.74	8.27	0.27
BU07-42-z3	2.73	2.49	7.76	0.23	4.05	43.25	673	614	0.91	34.22	0.75	10.37	0.31
weighted mean												9.42	0.17
BU07-43B-z1	2.42	1.50	7.47	0.25	3.90	49.25	619	385	0.62	28.62	0.78	9.60	0.32
BU07-43B-z2	1.12	0.81	7.45	0.24	2.41	39.25	466	337	0.72	21.91	0.73	10.15	0.33
BU07-43B-z3	4.56	4.09	6.89	0.21	6.40	56.25	713	639	0.90	32.10	0.81	8.55	0.26
weighted mean												9.28	0.17
BU07-53-z1	2.76	3.26	8.45	0.29	15.67	58.25	176	208	1.18	10.28	0.83	10.22	0.35
BU07-53-z2	2.27	2.59	6.53	0.21	13.36	62.00	170	194	1.14	7.58	0.83	7.88	0.25
BU07-53-z3	1.64	1.29	6.39	0.19	6.83	59.25	240	188	0.79	9.79	0.81	7.86	0.24
weighted mean												8.33	0.16
BU07-54-z1	8.22	6.71	6.72	0.22	29.99	78.00	274	224	0.82	11.83	0.86	7.78	0.26
BU07-54-z2	0.77	1.07	5.80	0.19	4.29	50.50	180	249	1.38	7.48	0.78	7.43	0.25
BU07-54-z3	0.84	0.50	5.98	0.19	7.84	45.50	108	64	0.59	3.96	0.79	7.62	0.25
weighted mean												7.60	0.14
BU07-55-z2	0.86	0.55	4.90	0.17	2.28	34.25	378	240	0.63	11.47	0.71	6.94	0.23
BU07-55-z3	1.96	3.22	10.53	0.28	2.14	33.00	915	1502	1.64	72.16	0.69	15.21	0.41
weighted mean												8.97	0.20
NBH-11-z1	0.92	0.09	4.70	0.19	1.54	29.00	596	61	0.10	15.47	0.67	7.03	0.28
NBH-11-z2	0.87	0.21	4.39	0.16	1.57	39.00	553	132	0.24	13.80	0.72	6.12	0.23
weighted mean												6.48	0.18
NBH-18-z2	2.89	1.61	9.57	0.33	8.30	62.00	349	195	0.56	20.37	0.82	11.62	0.40
NBH-18-z3	3.88	1.92	9.15	0.29	4.55	51.75	853	422	0.50	47.01	0.79	11.59	0.37
weighted mean												11.60	0.27

Table S3: Apatite fission-track ages and supporting data

Sample	Number of grains	Spontaneous Track Density $\rho_s \times 10^6 \text{ cm}^{-2}$ (Ns)	Induced Track Density $\rho_i \times 10^6 \text{ cm}^{-2}$ (Ni)	Dosimeter $\rho d \times 10^6 \text{ cm}^{-2}$ (Nd)	P(χ^2) (%)	Central Age $\pm 1\sigma$ (Ma)	U (ppm)
BU07-11	21	0.253 (39)	16.972 (2617)	1.637 (8557)	97.2	4.52 ± 0.73	22
BU07-12	10	0.391 (12)	33.891 (1040)	1.6104 (8557)	47.6	3.44 ± 1.00	54
BU07-27	15	0.415 (34)	28.893 (2368)	1.4879 (8557)	45.8	3.96 ± 0.69	52
BU07-29	14	0.425 (26)	38.001 (2325)	1.4553 (8557)	57	3.01 ± 0.6	57
BU07-33	20	0.1421 (128)	5.1033 (4596)	1.103 (5343)	87.6	5.69 ± 0.52	66
BU07-35	13	0.1806 (89)	6.4055 (3156)	1.1145 (5343)	49.5	5.82 ± 0.64	87
BU07-37	13	0.0677 (30)	2.3108 (1024)	1.1549 (5343)	96.1	6.27 ± 1.17	33

Table S4: U-Pb zircon analyses by LA-MC-ICP-MS

Analysis	U (ppm)	Isotope ratios										Apparent ages (Ma)							
		206Pb	U/Th	206Pb*	±	207Pb*	±	206Pb*	±	error	206Pb*	±	207Pb*	±	206Pb*	±	Best age	±	
		204Pb		207Pb*	(%)	235U*	(%)	238U	(%)	corr.	238U*	(Ma)	235U	(Ma)	207Pb*	(Ma)	(Ma)	(Ma)	
BU0742-4	901	92	59.5	22.4072	47.7	0.0135	47.9	0.0022	4.7	0.10	14.1	0.7	13.6	6.5	-75.9	1199.0	14.1	0.7	
BU0742-61	2459	253	183.8	25.8700	20.8	0.0124	21.0	0.0023	2.9	0.14	15.0	0.4	12.5	2.6	-440.1	535.6	15.0	0.4	
BU0742-50	1557	165	84.7	20.6310	28.2	0.0158	28.4	0.0024	3.6	0.13	15.2	0.5	15.9	4.5	122.3	660.0	15.2	0.5	
BU0742-58	1663	206	113.8	24.8651	28.1	0.0135	28.3	0.0024	3.4	0.12	15.6	0.5	13.6	3.8	-337.0	714.1	15.6	0.5	
BU0742-1	1471	163	88.0	18.2445	21.8	0.0190	22.1	0.0025	3.5	0.16	16.2	0.6	19.2	4.2	404.5	483.5	16.2	0.6	
BU0742-21	1319	219	129.2	21.3563	24.0	0.0165	24.3	0.0026	3.7	0.15	16.5	0.6	16.6	4.0	40.3	566.0	16.5	0.6	
BU0742-49	2368	204	99.4	22.8960	21.2	0.0156	21.4	0.0026	2.7	0.13	16.7	0.5	15.8	3.3	-128.9	515.8	16.7	0.5	
BU0742-37	1901	240	109.8	24.1801	21.4	0.0148	21.6	0.0026	3.1	0.14	16.7	0.5	15.0	3.2	-265.6	531.9	16.7	0.5	
BU0742-10	987	147	98.8	23.5330	39.1	0.0155	39.3	0.0027	4.2	0.11	17.1	0.7	15.7	6.1	-197.2	985.2	17.1	0.7	
BU0742-3	1615	182	87.6	18.6001	18.6	0.0200	18.9	0.0027	3.2	0.17	17.4	0.6	20.1	3.8	361.1	414.0	17.4	0.6	
BU0742-9	816	136	130.1	22.0191	38.6	0.0172	38.8	0.0027	4.6	0.12	17.7	0.8	17.3	6.7	-33.4	942.3	17.7	0.8	
BU0742-25	1282	204	122.3	25.2737	27.2	0.0160	27.4	0.0029	3.5	0.13	18.9	0.7	16.1	4.4	-379.2	695.7	18.9	0.7	
BU0742-51	2232	245	99.6	20.8928	17.4	0.0197	17.6	0.0030	2.6	0.15	19.3	0.5	19.8	3.5	92.5	404.2	19.3	0.5	
BU0742-19	1189	175	100.6	18.7167	21.3	0.0221	21.6	0.0030	3.6	0.17	19.3	0.7	22.1	4.7	347.0	475.1	19.3	0.7	
BU0742-13	1355	122	37.8	20.2933	24.0	0.0211	24.2	0.0031	3.2	0.13	20.0	0.6	21.2	5.1	161.0	554.3	20.0	0.6	
BU0742-28	1692	158	87.3	27.0492	27.3	0.0159	27.4	0.0031	2.9	0.11	20.1	0.6	16.0	4.4	-558.7	722.8	20.1	0.6	
BU0742-40	1473	213	107.3	23.0921	22.2	0.0195	22.5	0.0033	3.1	0.14	21.0	0.7	19.6	4.4	-150.1	542.7	21.0	0.7	
BU0742-14	1063	84	123.1	17.2049	23.5	0.0298	23.7	0.0037	3.2	0.13	23.9	0.8	29.8	7.0	534.4	509.8	23.9	0.8	
BU0742-56	1362	271	83.1	19.2243	15.8	0.0272	16.1	0.0038	3.1	0.19	24.4	0.7	27.3	4.3	286.2	354.7	24.4	0.7	
BU0742-15	531	265	133.3	23.7824	22.7	0.0224	23.2	0.0039	5.1	0.22	24.8	1.3	22.5	5.2	-223.7	560.8	24.8	1.3	
BU0742-30	1939	311	136.1	17.7033	10.5	0.0317	10.8	0.0041	2.4	0.23	26.2	0.6	31.7	3.4	471.5	227.7	26.2	0.6	
BU0742-20	755	252	40.2	18.9016	18.1	0.0424	18.4	0.0058	3.3	0.18	37.4	1.2	42.2	7.6	324.7	403.9	37.4	1.2	
BU0742-46	1287	263	128.3	22.3343	13.9	0.0378	14.1	0.0061	2.4	0.17	39.4	1.0	37.7	5.2	-67.9	331.6	39.4	1.0	
BU0742-60	1088	408	55.1	20.8925	12.2	0.0422	12.5	0.0064	2.7	0.21	41.1	1.1	42.0	5.1	92.5	283.4	41.1	1.1	
BU0742-47	1816	413	79.3	20.4154	9.2	0.0447	9.4	0.0066	2.0	0.21	42.5	0.8	44.4	4.1	147.0	210.7	42.5	0.8	
BU0742-34	1652	200	118.9	19.2647	5.2	0.0484	5.6	0.0068	2.0	0.36	43.4	0.9	48.0	2.6	281.4	116.1	43.4	0.9	
BU0742-38	1804	473	82.6	23.3097	9.2	0.0409	9.4	0.0069	1.9	0.21	44.4	0.9	40.7	3.7	-173.4	222.5	44.4	0.9	
BU0742-8	1152	373	47.7	20.6839	10.7	0.0480	11.0	0.0072	2.4	0.22	46.3	1.1	47.6	5.1	116.2	247.5	46.3	1.1	
BU0742-62	730	256	25.3	23.7218	19.8	0.0428	20.0	0.0074	3.0	0.15	47.3	1.4	42.6	8.3	-217.3	487.2	47.3	1.4	
BU0742-6	1038	253	56.7	24.3832	8.5	0.0460	8.8	0.0081	2.3	0.26	52.2	1.2	45.6	3.9	-286.9	211.4	52.2	1.2	
BU0742-23	858	272	22.5	24.3458	14.6	0.0485	14.8	0.0086	2.5	0.17	54.9	1.4	48.1	6.9	-283.0	361.9	54.9	1.4	
BU0742-39	1724	632	0.4	19.3362	5.8	0.0622	6.1	0.0087	1.8	0.29	55.9	1.0	61.2	3.6	272.9	129.9	55.9	1.0	
BU0742-54	1105	492	47.2	19.3856	8.1	0.0764	8.3	0.0107	2.0	0.24	68.9	1.4	74.7	6.0	267.0	181.1	68.9	1.4	
BU0742-57	706	146	69.7	17.5307	15.1	0.0855	15.3	0.0109	2.4	0.16	69.7	1.7	83.3	12.2	493.2	327.3	69.7	1.7	
BU0742-41	1243	9263	7.8	22.4899	2.4	0.0667	3.0	0.0109	1.9	0.63	69.8	1.3	65.6	1.9	-84.9	56.1	69.8	1.3	
BU0742-31	1239	493	92.8	15.0629	4.8	0.1170	5.1	0.0128	1.7	0.34	81.9	1.4	112.4	5.5	818.6	99.2	81.9	1.4	
BU0742-18	850	258	144.3	17.6557	5.9	0.1041	6.2	0.0133	2.0	0.32	85.4	1.7	100.5	6.0	477.5	127.4	85.4	1.7	

BU0742-59	1103	12437	4.3	13.6136	1.3	0.1837	2.0	0.0181	1.6	0.78	115.9	1.8	171.2	3.2	1026.5	25.6	115.9	1.8
BU0742-42	1389	1151	37.1	16.0082	2.7	0.1668	3.0	0.0194	1.3	0.44	123.6	1.6	156.6	4.4	690.1	56.9	123.6	1.6
BU0742-36	1302	776	58.3	17.1751	3.9	0.1704	4.1	0.0212	1.3	0.32	135.4	1.8	159.8	6.1	538.2	83.3	135.4	1.8
BU0742-11	672	724	19.1	14.5472	4.1	0.2197	4.5	0.0232	1.7	0.39	147.7	2.6	201.6	8.1	891.0	83.1	147.7	2.6
BU0742-43	795	745	68.3	16.2636	3.9	0.2065	4.2	0.0244	1.6	0.38	155.2	2.4	190.6	7.3	656.3	81.8	155.2	2.4
BU0742-5	778	1047	34.5	13.2304	2.9	0.2547	3.3	0.0244	1.6	0.48	155.7	2.4	230.4	6.8	1084.0	56.7	155.7	2.4
BU0742-45	1048	458	50.5	14.9609	3.4	0.2397	3.6	0.0260	1.3	0.36	165.5	2.2	218.1	7.1	832.8	69.4	165.5	2.2
BU0742-35	1173	1201	12.1	14.3066	2.2	0.2532	2.5	0.0263	1.3	0.49	167.2	2.1	229.2	5.2	925.3	44.8	167.2	2.1
BU0742-48	819	758	9.8	16.4093	3.8	0.2398	4.0	0.0285	1.4	0.35	181.4	2.6	218.3	7.9	637.1	79.8	181.4	2.6
BU0742-7	1218	1922	33.8	13.7379	1.6	0.2975	2.0	0.0296	1.1	0.58	188.3	2.1	264.4	4.6	1008.1	32.0	188.3	2.1
BU0742-63	1279	1487	13.9	17.4222	2.2	0.2410	2.4	0.0305	1.1	0.46	193.4	2.1	219.3	4.8	506.8	46.5	193.4	2.1
BU0742-44	1657	2359	25.9	14.5630	1.3	0.3212	1.6	0.0339	0.9	0.59	215.1	2.0	282.8	3.9	888.7	25.8	215.1	2.0
BU0742-27	1150	1630	58.3	16.9784	1.8	0.2985	2.1	0.0368	1.1	0.50	232.7	2.4	265.2	5.0	563.3	39.4	232.7	2.4
BU0742-55	766	1289	47.5	14.1067	2.3	0.3773	2.7	0.0386	1.3	0.49	244.2	3.1	325.0	7.4	954.2	46.8	244.2	3.1
BU0742-29	1185	1113	14.1	13.6318	2.0	0.4383	2.2	0.0433	1.0	0.44	273.5	2.6	369.1	6.9	1023.8	39.7	273.5	2.6
BU0742-26	1019	2338	47.2	11.4076	1.0	0.6205	1.4	0.0513	1.0	0.71	322.7	3.0	490.1	5.3	1375.0	18.0	322.7	3.0
BU0742-52	611	1554	9.3	12.9148	1.9	0.5644	2.3	0.0529	1.2	0.55	332.1	4.0	454.4	8.3	1132.3	36.8	332.1	4.0
BU0742-17	628	2458	17.6	11.9850	1.4	0.6754	1.8	0.0587	1.2	0.63	367.7	4.1	524.0	7.5	1279.5	27.4	367.7	4.1
BU0742-2	369	1440	4.4	12.3740	1.1	1.7157	1.5	0.1540	1.0	0.65	923.2	8.3	1014.4	9.6	1216.9	22.0	1216.9	22.0
BU0742-22	921	4756	5.5	10.6100	0.6	1.2529	1.0	0.0964	0.8	0.77	593.4	4.3	824.7	5.5	1513.1	11.5	1513.1	11.5
BU0742-53	546	68000	1.6	10.3474	0.3	2.8637	0.8	0.2149	0.7	0.90	1254.9	7.9	1372.4	5.8	1560.3	6.1	1560.3	6.1
BU0742-24	868	3933	14.5	9.5462	0.7	1.1666	1.1	0.0808	0.8	0.78	500.7	4.0	785.0	5.9	1710.0	12.3	1710.0	12.3
BU0742-12	1004	1357	5.5	9.2215	0.8	1.0366	1.2	0.0693	0.8	0.72	432.1	3.5	722.2	6.0	1773.4	14.5	1773.4	14.5
BU0742-16	329	911	6.2	8.8107	1.4	1.6623	1.8	0.1062	1.2	0.66	650.8	7.4	994.3	11.5	1856.2	24.2	1856.2	24.2

Notes:

1. All uncertainties are reported at the 1-sigma level, and include only measurement errors. Systematic errors would increase age uncertainties by 1-2%.

2. U concentration and U/Th are calibrated relative to our Sri Lanka standard zircon, and are accurate to ~20%.

3. Common Pb correction is from 204Pb, with composition interpreted from Stacey and Kramers (1975) and uncertainties of 1.0 for 206Pb/ 204Pb, 0.3 for 207Pb/ 204Pb, and 2.0 for 208Pb/ 204Pb.

4. U/Pb and 206Pb/ 207Pb fractionation is calibrated relative to fragments of a large Sri Lanka zircon of 563±3.2 Ma (2-sigma) (Gehrels et al., 2008).

5. U decay constants and composition as follows: 238U = 9.8485 × 10 -10, 235U = 1.55125 × 10 -10, 238U/ 235U = 137.88

6. All zircons analyzed from BU07-42 were ablated with a 15 micron-diameter beam.

Table S5: results of exhumation rate modeling

Kuru Chu transect:

Sample	Analysis	Age and error (Ma)	T closure range (°C)	High exh. rate (for low error age) since cooling age (mm/yr)			High exhumation rate between analyses (mm/yr)			Low exh. rate (for high error age) since cooling age (mm/yr)			Low exhumation rate between analyses (mm/yr)			Exhumation rate (for center age) since cooling age (mm/yr)			Exh. rate between analyses (for center age) (mm/yr)			Between these two analyses:
				20°C/km	30°C/km	40°C/km	20°C/km	30°C/km	40°C/km	20°C/km	30°C/km	40°C/km	20°C/km	30°C/km	40°C/km	20°C/km	30°C/km	40°C/km	20°C/km	30°C/km	40°C/km	
BH-378: middle of MCT sheet	Peak T	23.4 ± 1.2 ⁶	750-800 ¹	1.80	1.20	0.90	1.78	1.20	0.90	1.52	1.02	0.76	1.48	1.00	0.74	1.66	1.10	0.83	1.63	1.12	0.81	Peak T to ZHe
	ZHe	4.05 ± 0.07	194-198	1.9	1.2	0.9	1.90	1.20	0.90	1.75	1.10	0.85	1.75	1.10	0.85	1.8	1.05	0.9	1.80	1.05	0.90	ZHe to surface
BH-38: base of MCT sheet	Peak T	23.4 ± 1.2 ⁶	650 ¹	1.46	0.98	0.73	1.47	1.00	0.74	1.32	0.88	0.66	1.30	0.88	0.66	1.39	0.93	0.69	1.39	0.93	0.69	Peak T to ZHe
	ZHe	5.49 ± 0.12	191-194	1.45	0.9	0.7	1.45	0.90	0.70	1.4	0.9	0.65	1.40	0.90	0.65	1.4	0.9	0.7	1.40	0.90	0.70	ZHe to surface
BH-386: top of MCT sheet	Peak T	23.4 ± 1.2 ⁶	750-800 ¹	1.80	1.20	0.90	1.59	1.36	1.06	1.52	1.02	0.76	1.08	0.98	0.77	1.66	1.10	0.83	1.31	1.16	0.91	Peak T to MAr
	MAr	11.7 ± 0.2 ⁸	324-400	2.00	1.05	0.75	2.91	1.41	0.93	2.00	1.05	0.75	2.97	1.41	0.99	2.00	1.05	0.75	2.91	1.41	0.93	MAr to ZHe
BH-102: middle of MCT sheet	ZHe	6.42 ± 0.11	190-192	1.25	0.75	0.6	1.25	0.75	0.60	1.2	0.75	0.55	1.20	0.75	0.55	1.25	0.75	0.6	1.25	0.75	0.60	ZHe to surface
	AFT	6.5 ± 0.6 ⁴	118-121	0.8	0.5	0.5	0.80	0.50	0.50	0.65	0.45	0.3	0.65	0.45	0.30	0.7	0.5	0.35	0.70	0.50	0.35	AFT to surface
BH-101: low in MCT sheet	Peak T	23.4 ± 1.2 ⁶	750-800 ¹	1.80	1.20	0.90	2.30	1.56	1.17	1.52	1.02	0.76	1.83	1.24	0.93	1.66	1.10	0.83	2.05	1.38	1.04	Peak T to ZHe
	ZHe	8.37 ± 0.13	187-190	0.95	0.6	0.45	1.25	0.70	0.55	0.95	0.6	0.45	1.88	1.16	0.82	0.95	0.6	0.45	1.49	0.87	0.58	ZHe to AFT
BU07-6: top of northern lower LH sheet	AFT	6.1 ± 0.6 ⁴	119-121	0.8	0.55	0.4	0.80	0.55	0.40	0.7	0.45	0.35	0.70	0.45	0.35	0.75	0.5	0.4	0.75	0.50	0.40	AFT to surface
	ZHe	5.62 ± 0.12	191-194	1.45	0.9	0.7	1.45	0.90	0.70	1.4	0.9	0.65	1.40	0.90	0.65	1.4	0.9	0.7	1.40	0.90	0.70	ZHe to surface
NBH-11: middle of northern lower LH sheet	Peak T	ca. 20-22 ¹	450-500 ²	1.25	0.83	0.63	0.23	0.42	0.33	1.02	0.68	0.51	-0.03	0.24	0.23	1.13	0.75	0.57	0.12	0.32	0.28	Peak T to MAr
	MAr	8.40 ± 0.77	328-409	2.9	1.5	1.1	6.64	3.05	2.13	2.5	1.3	0.9	4.34	1.97	1.32	2.65	1.4	1	5.18	2.41	1.61	MAr to ZHe
BU07-9: base of northern lower LH sheet	ZHe	5.62 ± 0.12	191-194	1.45	0.9	0.7	1.45	0.90	0.70	1.4	0.9	0.65	1.40	0.90	0.65	1.4	0.9	0.7	1.40	0.90	0.70	ZHe to surface
	MAr	9.18 ± 0.17	328-405	2.5	1.25	0.95	5.41	2.41	1.76	2.4	1.3	0.9	5.37	2.66	1.77	2.5	1.3	0.9	5.50	2.62	1.62	MAr to ZHe
BU07-9: base of northern lower LH sheet	AFT	6.48 ± 0.18	190-192	1.25	0.75	0.6	1.25	0.75	0.60	1.2	0.75	0.55	1.20	0.75	0.55	1.25	0.75	0.6	1.25	0.75	0.60	ZHe to surface
	ZHe	6.70 ± 0.13	190-192	1.25	0.75	0.6	1.25	0.75	0.60	1.2	0.75	0.55	1.20	0.75	0.55	1.25	0.75	0.6	1.25	0.75	0.60	ZHe to surface
BU07-11: top of ST sheet	Peak T	ca. 20-22 ¹	450-500 ²	1.45	0.97	0.73	0.39	0.81	0.68	1.13	0.75	0.56	-0.08	0.36	0.35	1.28	0.85	0.64	0.03	0.51	0.45	Peak T to MAr
	MAr	11.78 ± 0.41	324-400	2	1.05	0.75	3.37	1.61	1.07	1.9	1	0.7	3.10	1.45	0.92	2	1.05	0.75	3.39	1.59	1.06	MAr to ZHe
BU07-11: top of ST sheet	ZHe	7.16 ± 0.15	189-191	1.15	0.7	0.55	1.09	0.58	0.49	1.1	0.7	0.55	1.61	0.95	0.80	1.1	0.7	0.55	1.27	0.79	0.64	ZHe to AFT
	AFT	4.52 ± 0.73	123-125	1.2	0.8	0.6	1.20	0.80	0.60	0.9	0.6	0.45	0.90	0.60	0.45	1	0.65	0.5	1.00	0.65	0.50	AFT to surface
BU07-12: middle of ST sheet	Peak T	ca. 20 ¹ -17.2	400-500 ²	1.45	0.97	0.73	0.39	0.81	0.68	1.13	0.75	0.56	-0.08	0.36	0.35	1.28	0.85	0.64	-0.08	0.45	0.43	Peak T to MAr
	MAr	12.11 ± 0.46	323-400	2	1.05	0.75	4.75	2.23	1.54	1.85	0.95	0.7	3.93	1.76	1.28	1.9	1	0.7	4.23	1.98	1.31	MAr to ZHe
BU07-12: middle of ST sheet	ZHe	8.60 ± 0.17	187-190	0.95	0.6	0.45	0.64	0.42	0.27	0.95	0.6	0.45	0.85	0.50	0.40	0.95	0.6	0.45	0.75	0.43	0.32	ZHe to AFT
	AFT	3.44 ± 1.00	123-129	1.7	1.05	0.9	1.70	1.05	0.90	1.05	0.7	0.5	1.05	0.70	0.50	1.25	0.85	0.65	1.25	0.85	0.65	AFT to surface
BH-342: middle of ST sheet	Peak T	ca. 20 ¹ -17.2	400-500 ²	1.45	0.97	0.73	1.94	1.32	0.99	1.00	0.67	0.50	1.04	0.72	0.54	1.21	0.81	0.60	1.43	0.98	0.74	Peak T to ZHe
	ZHe	8.55 ± 0.14	187-190	0.95	0.6	0.45	0.95	0.60	0.45	0.95	0.6	0.45	0.95	0.60	0.45	0.95	0.6	0.45	0.95	0.60	0.45	ZHe to surface
BU07-13: base of ST sheet	Peak T	ca. 20 ¹ -17.2	400-500 ²	1.45	0.97	0.73	2.25	1.52	1.16	1.00	0.67	0.50	1.21	0.84	0.60	1.21	0.81	0.60	1.63	1.16	0.84	Peak T to ZHe
	ZHe	9.97 ± 0.20	185-188	0.85	0.55	0.4	0.85	0.55	0.40	0.8	0.5	0.4	0.80	0.50	0.40	0.85	0.5	0.4	0.85	0.50	0.40	ZHe to surface
BU07-21: base of ST sheet (Daling Fm. Klippe)	Peak T	ca. 20 ¹ -17.2	<ca. 400 ¹⁰	1.16	0.78	0.58	1.37	0.94	0.71	1.00	0.67	0.50	1.04	0.72	0.54	1.08	0.72	0.54	1.18	0.82	0.61	Peak T to ZHe
	ZHe	8.62 ± 0.16	187-190	0.95	0.6	0.45	0.95	0.60	0.45	0.95	0.6	0.45	0.95	0.60	0.45	0.95	0.6	0.45	0.95	0.60	0.45	ZHe to surface
BU07-14: Baxa Group horse #2	Peak T	14.8 ± 0.3	350 ³	1.21	0.80	0.60	1.78	1.28	0.98	1.16	0.77	0.58	1.73	1.18	0.91	1.18	0.79	0.59	1.71	1.23	0.95	Peak T to ZHe
	ZHe	9.62 ± 0.17	186-188	0.9	0.55	0.4	0.90	0.55	0.40	0.85	0.55	0.4	0.85	0.55	0.40	0.9	0.55	0.4	0.90	0.55	0.40	ZHe to surface
BU07-18: Baxa Group horse #1	Peak T	14.8 ± 0.3	350 ³	1.21	0.80	0.60	1.79	1.29	0.99	1.16	0.77	0.58	1.74	1.19	0.92	1.18	0.79	0.59	1.72	1.24	0.95	Peak T to ZHe
	ZHe	9.68 ± 0.19	186-188	0.9	0.55	0.4	0.90	0.55	0.40	0.85	0.55	0.4	0.85	0.55	0.40	0.9	0.55	0.4	0.90	0.55	0.40	ZHe to surface
BU07-22: Baxa Group horse #1	Peak T	14.78 ± 0.34 ⁹	ca. 400 ⁹	1.39	0.92	0.69	2.45	1.67	1.28	1.32	0.88	0.66	2.35	1.63	1.17	1.35	0.90	0.68	2.35	1.70	1.22	Peak T to ZHe
	ZHe	9.82 ± 0.20	185-188	0.85	0.55	0.4	0.85	0.55	0.40	0.8	0.5	0.4	0.80	0.50	0.40	0.85	0.5	0.4	0.85	0.50	0.40	ZHe to surface
BU07-24: Baxa Group horse#7	Peak T	14.8 ± 0.3	350 ³	1.21	0.80	0.60	1.55	1.08	0.81	1.16	0.77	0.58	1.45	1.01	0.76	1.18	0.79	0.59	1.50	1.04	0.78	Peak T to ZHe
	ZHe	8.52 ± 0.21	187-190	0.95	0.6	0.45	0.95	0.60	0.45	0.95	0.6	0.45	0.95	0.60	0.45	0.95	0.6	0.45	0.95	0.60	0.45	ZHe to surface

BU07-26: Baxa Group horse #8	Peak T ZHe modern	14.8 ± 0.3 9.86 ± 0.20	350^3 $185-188$	1.21 0.85	0.80 0.55	0.60 0.4	1.92 0.85	1.31 0.55	1.01 0.40	1.16 0.8	0.77 0.5	0.58 0.4	1.88 0.80	1.32 0.50	0.94 0.40	1.18 0.85	0.79 0.5	0.59 0.4	1.85 0.85	1.36 0.50	0.97 Peak T to ZHe 0.40 ZHe to surface	
BU07-27: top of Diuri Fm. Sheet	Peak T ZHe AFT modern	timing of achieve 250-310 ² 8.86 ± 0.16 3.96 ± 0.69	$186-189$ $122-127$	0.95 1.3	0.6 0.9	0.45 0.7	0.74 1.30	0.42 0.90	0.30 0.70	0.9 0.95	0.6 0.65	0.45 0.5	0.85 0.95	0.55 0.65	0.40 0.50	0.95 1.1	0.95 0.75	0.6 0.6	0.45 0.45	0.83 1.10	0.48 0.75	0.33 ZHe to AFT 0.60 AFT to surface
BU07-29: base of Diuri Fm. Sheet	Peak T ZHe AFT modern	timing of achieve 250-310 ² 7.50 ± 0.13 3.01 ± 0.60	$188-191$ $124-129$	1.1 1.7	0.7 1.1	0.55 0.9	0.81 1.70	0.51 1.10	0.38 0.90	1.05 1.2	0.65 0.8	0.5 0.6	0.92 1.20	0.52 0.80	0.41 0.60	1.1 1.4	0.75 0.95	0.6 0.75	0.90 1.40	0.62 0.95	0.50 ZHe to AFT 0.75 AFT to surface	

Trashigang transect:

Sample	Analysis	Age and error (Ma)	T closure range (°C)	High exh. rate (for low error age) since cooling age (mm/yr)			High exhumation rate between analyses (mm/yr)			Low exh. rate (for high error age) since cooling age (mm/yr)			Low exhumation rate between analyses (mm/yr)			Exhumation rate (for center age) since cooling age (mm/yr)			Exh. rate between analyses (for center age) (mm/yr)			Between these two analyses		
				20°C/km	30°C/km	40°C/km	20°C/km	30°C/km	40°C/km	20°C/km	30°C/km	40°C/km	20°C/km	30°C/km	40°C/km	20°C/km	30°C/km	40°C/km	20°C/km	30°C/km	40°C/km	20°C/km	30°C/km	40°C/km
Top of GH section (samples just below KT)	Peak T AFT modern	23.4 ± 1.2^6 $3.84 \pm 0.27^{**}$	$750-800^1$ $123-126$	1.80 1.25	1.20 0.85	0.90 0.65	1.91 1.25	1.27 0.85	0.95 0.65	1.52 1.05	1.02 0.7	0.76 0.55	1.62 1.05	#VALUE! #VALUE!	0.80 0.55	1.66 1.15	1.10 0.75	0.83 0.6	1.76 1.15	1.17 0.75	0.87 Peak T to AFT 0.60 AFT to surface	0 20		
Upper GH section (samples between fold axes)	Peak T AFT modern	23.4 ± 1.2^6 $5.70 \pm 0.28^{**}$	$750-800^1$ $119-121$	1.80 0.85	1.20 0.55	0.90 0.4	2.11 0.85	1.41 0.55	1.06 0.40	1.52 0.75	1.02 0.5	0.76 0.4	1.77 0.75	1.18 0.50	0.88 0.40	1.66 0.7	1.10 0.5	0.83 0.4	1.96 0.70	1.30 0.50	0.97 Peak T to AFT 0.40 AFT to surface	0 20		
Mid-GH section (samples near Trashigang)	Peak T MAr ZHe AFT modern	23.4 ± 1.2^6 11.1 ± 0.2^5 7.09 ± 0.14 $3.4 \pm 0.41^{**}$	$750-800^1$ $325-401$ $189-191$ $124-127$	1.80 2.15 1.15 1.4	1.20 0.8 0.7 0.95	0.90 3.91 0.51 0.40	1.91 1.80 0.96 1.40	1.27 1.24 1.1 1.05	0.95 2.05 1.1 0.75	1.52 1.1 0.55 0.75	1.02 1.1 0.55 0.75	0.76 0.64 0.49 0.6	1.62 3.74 1.04 1.15	#VALUE! 1.81	0.80 1.11	1.66 2.1	1.10 1.1	0.83 0.55	1.76 0.96	1.17 0.56	0.85 Peak T to MAr 1.24 MAr to ZHe 0.46 Zhe to AFT 0.65 AFT to surface	0 20		
Low in GH section (between MCT and Trashigang)	Peak T MAr	23.4 ± 1.2^6 14.1 ± 0.2^5	$750-800^1$ $322-397$	1.80 1.7	1.20 0.9	0.90 0.65	1.97 1.70	1.71 0.90	1.32 0.65	1.52 1.7	1.02 0.85	0.76 0.6	1.28 1.70	1.25 0.85	0.99 0.60	1.66 1.7	1.10 0.9	0.83 0.6	1.59 1.70	1.41 0.90	1.17 Peak T to MAr 0.60 MAr to surface	0 20		
BH-78: base of Chekha Fm.	Peak T ZHe AFT modern	21.6 ± 0.6^6 7.09 ± 0.14 $5.68 \pm 0.29^{**}$	650^7 $189-191$ $119-122$	1.55 1.15 0.85	1.03 0.7 0.55	0.77 2.19 0.45	1.74 2.19	1.20 1.22	0.88 0.90	1.46 1.1	0.98 0.7	0.73 0.55	1.64 2.76	1.11 1.65	0.82 1.26	1.50 1.1	1.00 0.7	0.75 0.55	1.70 2.31	1.15 1.30	0.85 Peak T to ZHe 1.15 Zhe to AFT 0.40 AFT to surface	0 20		
BU07-55: top of ST sheet	Peak T MAr ZHe AFT modern	ca. $20^1-17.2$ 13.5 ± 0.1^5 8.97 ± 0.20 $4.3 \pm 0.51^{**}$	$450-510^3$ $323-397$ $186-189$ $122-125$	1.48 1.8 0.95 1.15	0.99 0.9 0.6 0.8	0.74 0.65 0.45 0.6	0.36 3.41 0.80 1.15	1.30 1.47 0.45 0.80	1.06 1.03 0.9 0.60	1.13 1.8 0.9 0.95	0.75 0.65 0.45 0.6	0.56 0.5 0.45 0.45	-0.31 3.66 0.84 0.95	0.43 1.52 0.60 0.60	0.38 1.06 0.45 0.45	1.29 1.8 1.05 1.05	0.86 0.9 0.7 0.7	0.65 0.65 0.45 0.5	-0.06 3.48 0.86 1.05	0.75 1.49 0.51 0.70	0.63 Peak T to MAr 1.05 MAr to ZHe 0.40 Zhe to AFT 0.50 AFT to surface	0 20		
BH-57: middle of ST sheet	Peak T ZHe AFT modern	ca. $20^1-17.2$ 7.26 ± 0.11 $4.93 \pm 0.31^{**}$	$450-510^3$ $189-191$ $121-123$	1.48 1.15 0.95	0.99 0.7 0.65	0.74 0.55 0.5	1.72 1.52 0.95	1.19 0.79 0.65	0.88 0.64 0.50	1.13 1.1 0.9	0.75 0.55 0.45	0.56 0.45 0.45	1.14 1.59 0.90	0.78 1.07 0.55	0.57 0.80	1.29 1.1	0.86 0.7	0.65 0.55	1.41 1.52	0.96 0.90	0.71 Peak T to ZHe 0.76 Zhe to AFT 0.45 AFT to surface	0 20		
BU07-43B: middle of ST sheet	Peak T ZHe modern	ca. $20^1-17.2$ 9.28 ± 0.17	$450-510^3$ $186-189$	1.48 0.9	0.99 0.55	0.74 0.45	2.14 0.90	1.48 0.55	1.07 0.9	1.13 0.55	0.75 0.4	0.56 0.4	1.33 0.90	0.93 0.55	0.71 0.40	1.29 0.9	0.86 0.55	0.65 0.4	1.68 0.90	1.17 0.55	0.89 Peak T to ZHe 0.40 ZHe to surface	0 20		
BU07-42: Baxa Group horse #3	Peak T ZHe modern	14.9 ± 0.7 9.42 ± 0.17	$400-450^2$ $186-188$	1.58 0.9	1.06 0.55	0.79 0.4	2.86 0.90	2.00 0.55	1.53 0.40	1.28 0.85	0.85 0.55	0.64 0.4	1.97 0.85	1.34 0.55	1.03 0.40	1.43 0.9	0.95 0.55	0.71 0.4	2.33 0.90	1.64 0.55	1.25 Peak T to ZHe 0.40 ZHe to surface	0 20		
BU07-37: Baxa Group horse #4	Peak T ZHe AFT modern	14.9 ± 0.7 11.24 ± 0.22 6.27 ± 1.17	350^3 $184-187$ $118-122$	1.23 0.75 0.9	0.82 0.55 0.6	0.62 0.35 0.45	2.90 0.62 0.90	1.94 0.41 0.60	1.54 0.26 0.45	1.12 0.75 0.65	0.75 0.45 0.4	0.56 0.35 0.3	2.15 0.94 0.65	1.57 0.54 0.40	1.14 0.44 0.30	1.17 0.75 0.75	0.78 0.5 0.5	0.59 0.35 0.35	2.48 0.75 0.75	1.65 0.50 0.50	1.32 Peak T to ZHe 0.35 ZHe to AFT 0.35 AFT to surface	0 20		
NBH-18: Baxa Group horse #5	Peak T ZHe modern	14.9 ± 0.7 11.60 ± 0.27	350^3 $184-187$	1.23 0.75	0.82 0.55	0.62 0.35	3.14 0.75	1.89 0.55	1.67 0.7 0.55	1.12 0.55 0.35	0.75 0.35 0.3	0.56 0.35 0.3	2.46 1.05 0.70	1.38 0.55 0.55	1.23 0.35 0.35	1.17 0.55 0.55	0.78 0.35 0.35	0.59 0.35 0.35	2.84 0.70 0.70	1.60 0.55 0.55	1.42 Peak T to ZHe 0.35 ZHe to surface	0 20		
BU07-36: Baxa Group horse #6	Peak T ZHe modern	14.9 ± 0.7 10.80 ± 0.21	350^3 $184-187$	1.23 0.8	0.82 0.5	0.62 0.35	2.50 0.80	1.77 0.50	1.40 0.35	1.12 0.75	0.75 0.5	0.56 0.35	2.01 0.75	1.34 0.50	1.07 0.35	1.17 0.8	0.78 0.5	0.59 0.35	2.16 0.80	1.53 0.50	1.21 Peak T to ZHe 0.35 ZHe to surface	0 20		
BU07-35: Baxa Group horse #7	Peak T ZHe AFT modern	14.9 ± 0.7 10.48 ± 0.20 5.82 ± 0.64	350^3 $184-187$ $119-122$	1.23 0.8 0.9	0.82 0.5 0.6	0.62 0.35 0.45	2.37 0.70 0.90	1.66 0.40 0.60	1.31 0.26 0.45	1.12 0.75 0.45	0.75 0.5 0.45	0.56 0.35 0.35	1.93 0.83 0.70	1.29 0.58 0.45	1.02 0.35 0.35	1.17 0.8 0.8	0.78 0.5 0.5	0.59 0.35 0.4	2.06 0.80	1.45 0.50	1.15 Peak T to ZHe 0.29 ZHe to AFT 0.40 AFT to surface	0 20		
BU07-33: top of Diuri Fm. Sheet	Peak T ZHe AFT modern	timing of achieve 250-310 ² 11.16 ± 0.23 5.69 ± 0.52	$184-187$	0.75 0.9	0.5 0.6	0.35 0.45	0.62 0.90	0.41 0.60	0.26 0.45	0.75 0.7 0.45	0.45 0.45	0.35 0.35	0.81 0.70	0.45 0.45	0.35 0.35	0.75 0.8	0.5 0.5	0.35 0.4	0.70 0.80	0.50 0.50	0.30 Peak T to ZHe 0.40 AFT to surface	0 20		

BU07-54: base of Diuri Fm. Sheet	Peak T ZHe modern	timing of achieve 250-310 ² 7.60 ± 0.14 188-191	1.1 0.7 0.55	1.10	0.70	0.55	1.05 0.65 0.5	1.05 0.65 0.50	1.1 0.75 0.6	1.10	0.75	Peak T to ZHe 0.60 ZHe to surface
BU07-53: top of MBT sheet (Gondwana succ.)	Peak T ZHe modern	timing of achieve 250-310 ² 8.33 ± 0.16 187-190	0.95 0.6 0.45	0.95	0.60	0.45	0.95 0.6 0.45	0.95 0.60 0.45	0.95 0.95 0.6 0.45	0.95	0.60	Peak T to ZHe 0.45 ZHe to surface

*Weighted mean of 2 ages, **Weighted mean of 3 ages
Data sources: ¹ Daniel et al. (2003), ² Long et al. (2011C), ³ Whynot et al. (2010), ⁴ Grujic et al. (2006), ⁵ Stüwe and Foster (2001), ⁶ Chambers et al. (2011), ⁷ Kellett et al. (2010), ⁸ Kellett et al. (2009),
⁹ 400°C def. temp. from quartz microstructure (Fig. 4; Stipp et al., 2002); time of peak T is 14.8±0.3 Ma MAr age, ¹⁰ ca. 400°C maximum temp. because not reset for MAr